RESEARCH ARTICLE

Global Change Biology WILEY

Microbial methane cycling in sediments of Arctic thermokarst lagoons

Sizhong Yang[1,2] | Sara E. Anthony[3] | Maren Jenrich[4,5] | Michiel H. in 't Zandt[6,7] | Jens Strauss[4] | Pier Paul Overduin[4] | Guido Grosse[4,5] | Michael Angelopoulos[4] | Boris K. Biskaborn[8] | Mikhail N. Grigoriev[9] | Dirk Wagner[1,5] | Christian Knoblauch[10,11] | Andrea Jaeschke[3] | Janet Rethemeyer[3] | Jens Kallmeyer[1] | Susanne Liebner[1,12]

[1]GFZ German Research Center for Geosciences, Helmholtz Centre Potsdam, Section Geomicrobiology, Potsdam, Germany

[2]Cryosphere Research Station on the Qinghai-Tibet Plateau, State Key Laboratory of Cryospheric Science, Northwest Institute of Eco-Environment and Resources, Chinese Academy of Sciences, Lanzhou, China

[3]Institute of Geology and Mineralogy, University of Cologne, Cologne, Germany

[4]Permafrost Research Section, Alfred Wegener Institute Helmholtz Center for Polar and Marine Research, Potsdam, Germany

[5]Institute of Geosciences, University of Potsdam, Potsdam, Germany

[6]Department of Microbiology, RIBES, Radboud University, Nijmegen, the Netherlands

[7]Netherlands Earth System Science Center, Utrecht University, Utrecht, the Netherlands

[8]Polar Terrestrial Environmental Systems Section, Alfred Wegener Institute Helmholtz Center for Polar and Marine Research, Potsdam, Germany

[9]Laboratory of General Geocryology, Melnikov Permafrost Institute, Siberian Branch of the Russian Academy of Sciences, Yakutsk, Russia

[10]Institute of Soil Science, Universität Hamburg, Hamburg, Germany

[11]Center for Earth System Research and Sustainability, Universität Hamburg, Hamburg, Germany

[12]Institute of Biochemistry and Biology, University of Potsdam, Potsdam, Germany

Correspondence
Sizhong Yang, GFZ German Research Center for Geosciences, Helmholtz Centre Potsdam, Section Geomicrobiology, Telegrafenberg, 14473 Potsdam, Germany.
Email: syang@gfz-potsdam.de

Sara E. Anthony, Department of Landscape Ecology, University of Rostock, 18059 Rostock, Germany.
Email: sara.anthony@uni-rostock.de

Susanne Liebner, Institute of Biochemistry and Biology, University of Potsdam, 14476 Potsdam, Germany.
Email: sliebner@gfz-potsdam.de

Present address
Sara E. Anthony, Department of Landscape Ecology, Faculty of Agricultural and Environmental Sciences, University of Rostock, Rostock, 18059 Germany

Abstract

Thermokarst lagoons represent the transition state from a freshwater lacustrine to a marine environment, and receive little attention regarding their role for greenhouse gas production and release in Arctic permafrost landscapes. We studied the fate of methane (CH_4) in sediments of a thermokarst lagoon in comparison to two thermokarst lakes on the Bykovsky Peninsula in northeastern Siberia through the analysis of sediment CH_4 concentrations and isotopic signature, methane-cycling microbial taxa, sediment geochemistry, lipid biomarkers, and network analysis. We assessed how differences in geochemistry between thermokarst lakes and thermokarst lagoons, caused by the infiltration of sulfate-rich marine water, altered the microbial methane-cycling community. Anaerobic sulfate-reducing ANME-2a/2b methanotrophs dominated the sulfate-rich sediments of the lagoon despite its known seasonal alternation between brackish and freshwater inflow and low sulfate concentrations compared to the usual marine ANME habitat. Non-competitive methylotrophic methanogens dominated the methanogenic community of the lakes and

Michiel H. in 't Zandt, Soil Biology Group, Wageningen University, Wageningen, the Netherlands

the lagoon, independent of differences in porewater chemistry and depth. This potentially contributed to the high CH_4 concentrations observed in all sulfate-poor sediments. CH_4 concentrations in the freshwater-influenced sediments averaged $1.34 \pm 0.98 \, \mu mol \, g^{-1}$, with highly depleted δ^{13}C-CH_4 values ranging from −89‰ to −70‰. In contrast, the sulfate-affected upper 300 cm of the lagoon exhibited low average CH_4 concentrations of $0.011 \pm 0.005 \, \mu mol \, g^{-1}$ with comparatively enriched δ^{13}C-CH_4 values of −54‰ to −37‰ pointing to substantial methane oxidation. Our study shows that lagoon formation specifically supports methane oxidizers and methane oxidation through changes in pore water chemistry, especially sulfate, while methanogens are similar to lake conditions.

KEYWORDS
^{13}C, ANME, AOM, coastal permafrost, methanotrophs, methylotrophic methanogenesis, MOB, permafrost thaw, sulfate-methane transition zone, sulfate reduction

1 | INTRODUCTION

Northern permafrost contains an estimated 1035 ± 150 PG of organic carbon within the top three meters (Hugelius et al., 2014), which is more than 30% of total terrestrial soil organic carbon (Strauss et al., 2021) and disproportionally high, given its limited coverage of 15%–22% of the terrestrial area (Schuur et al., 2015). The warming climate has triggered permafrost degradation with a variety of consequences for the landscape (Biskaborn et al., 2019), including top-down thaw, increasing active layer over long term, thermo-erosion along coasts, rivers, and lake shores, rapid thawing associated with thermokarst processes (Strauss et al., 2017; Turetsky et al., 2020) and significant land subsidence (Anders et al., 2020; Antonova et al., 2018). Thermokarst develops in the lowland areas of ice-rich permafrost, and typically results in formation of thermokarst ponds or lakes (Bouchard et al., 2016) and reassembly of permafrost microbiomes (Ernakovich et al., 2022). Thermokarst landscapes are estimated to cover approximately 20%–40% of permafrost regions (Olefeldt et al., 2016; Strauss et al., 2017). Thermokarst lakes are hotspots of CH_4 emission (Pellerin et al., 2022; Walter Anthony et al., 2016), especially those lakes that formed in organic-rich Yedoma permafrost, which contains approximately 40% of total permafrost carbon. As CH_4 *has* approximately 34 times the global warming potential of carbon dioxide (CO_2) over 100 years (Dean et al., 2018; Myhre et al., 2013), excessive CH_4 emissions from thermokarst landscapes can yield disproportionate CO_2 equivalents and feedback to the climate system (Serikova et al., 2019; Walter Anthony et al., 2018).

Marine systems only contribute 1%–2% of global CH_4 emissions even though they cover approximately 70% of the earth's surface, due to effective reduction of CH_4 emissions through anaerobic methane oxidation coupled with sulfate reduction termed S-AOM (Hinrichs & Boetius, 2002; Knittel et al., 2019; Wallenius et al., 2021). S-AOM consortia, symbiosis between anaerobic methanotrophic archaea (ANMEs) and sulfate-reducing bacteria, are widespread in marine systems, although ANMEs are very slow growing (Knittel & Boetius, 2009). There are three main clades of marine ANMEs: ANME-1, ANME-2 (further split into subclusters ANME-2a/2b and ANME-2c), and ANME-3. The differentiation between the clades is based on their relation to already cultivated methanogens, for example the ANME-2 clade is closely related to *Methanosarcinales* (Hinrichs et al., 1999; Knittel et al., 2005; Timmers et al., 2015). Because ANME organisms are ubiquitous in marine environments where CH_4 and sulfate are present, they potentially also establish in Arctic lagoons.

Thermokarst lagoons represent a transitional state between freshwater thermokarst lakes and a fully marine environment. The functionality of thermokarst lagoons in carbon turnover and greenhouse gas release has received little attention so far despite their importance in coastal carbon dynamics (In 't Zandt et al., 2020) and widespread occurrence along Arctic coasts (Angelopoulos et al., 2021). Lagoon formation occurs when intrusion of marine water introduces high concentrations of ions, especially sulfate, to the geochemical profiles of previous freshwater lakes (Spangenberg et al., 2021). Vertical diffusion of these salts also changes the ion composition of the freshwater sediments, creating a salt gradient across several meters of sediment (Angelopoulos et al., 2020). The sediment geochemistry of thermokarst lagoons largely depend on their hydrological connection with the sea. For example, open lagoons have a constant exchange with the sea leading to a more stable mixing regime and higher salinity and sulfate concentrations,

while semi-closed lagoons have a seasonal connection that is often interrupted during winter months due to ice thickening resulting in seasonally more variable environmental conditions (Jenrich et al., 2021; Schirrmeister et al., 2018).

One impact of marine-water intrusion could be a change in methane production pathway and the methanogenic community. Methanogenesis is accomplished through three main pathways: hydrogenotrophic, which utilizes hydrogen and carbon dioxide; acetoclastic, which utilizes acetate; and methylotrophic, which uses simple methylated compounds, such as methanol or methylamines (Liu & Whitman, 2008; Sollinger & Urich, 2019). Acetoclastic and hydrogenotrophic methanogenesis are more susceptible to competition (Froelich et al., 1979; Jørgensen, 2006), such as from sulfate reducing bacteria (SRB), whereas methylotrophic methanogens are thought to be non-competitive and therefore could continue under conditions unacceptable for the other two pathways (Liu & Whitman, 2008; Lyu et al., 2018). Indeed, recent studies have shown methylotrophic methanogenesis occurring in sulfate-rich areas, for example in the sulfate–methane transition zone of estuaries (Maltby et al., 2018; Sela-Adler et al., 2017).

We investigated sediments of two thermokarst lakes and a thermokarst lagoon on the Bykovsky Peninsula in northeastern Siberia as a natural laboratory for the impacts of marine-water intrusion on methane cycling through the analysis of sediment CH_4 concentrations and isotopic signature, methane-cycling microbial taxa, sediment geochemistry, and lipid biomarkers.

2 | MATERIALS AND METHODS

2.1 | Site description

The study area is located on the Bykovsky Peninsula, southeast of the Lena Delta in the Buor-Khaya Gulf of the Laptev Sea in northeastern Siberia, Russia (Figure 1). Three of the water bodies on the peninsula were selected for this study: two freshwater thermokarst lakes, Lake Golzovoye (also anglicized as Goltsovoye, abbreviated as LG in this study) and Northern Polar Fox Lake (LNPF) and one thermokarst lagoon, Polar Fox Lagoon (PFL). Initial thermokarst lake formation occurred between 12,500 and 9400 years cal BP (calibrated, before present), before the peninsula itself was shaped (Grosse et al., 2007). Lake Golzovoye is relatively young, and formed approximately 8000 years cal BP (Jongejans et al., 2020). Northern Polar Fox Lake and Polar Fox Lagoon lie within the same partially drained thermokarst basin (Angelopoulos et al., 2020), with the lake to the north of the lagoon. The basin may have gone through repeated draining events between initial formation and present (Grosse et al., 2007; Jenrich, 2020). The channel between the lagoon and Tiksi Bay likely only formed within the last 2000 years cal BP. Thus, we view Northern Polar Fox Lake and Polar Fox Lagoon as two successive stages in the transition of coastal thermokarst landscapes into marine environments. The lagoon in its present state is a nearly closed system with a wide, shallow, and winding channel supplying it with water from

Tiksi Bay during the summer, with large seasonal variation in salinity and ion concentrations such as sulfate and chloride (Angelopoulos et al., 2020; Spangenberg et al., 2021). The mean annual electrical conductivity of Tiksi Bay is 7.1 mS cm^{-1}, but values as high as 15 mS cm^{-1} have been observed in winter (Angelopoulos et al., 2020).

2.2 | Field work and sampling

During a drilling campaign on the Bykovsky Peninsula in April 2017, cores PG2420, PG2426, and PG2423 were retrieved from LG, LNPF, and PFL, with drilling depths from the sediment surface of 5.2, 5.4, and 6.1 m, respectively. Water height above sediment surface was 510, 560, and 310 cm for LG, LNPF and PFL, respectively. The cores were recovered with a hammer-driven 60 mm Niederreiter piston corer (UWITEC™) in overlapping sections retrieved in 3-m-core barrels. All cores consisted of unfrozen sediment at time of sampling. After retrieval, the cores were cut into 10 cm liner segments. The cores were cut with an electric saw. To avoid contamination, the saw blade was wiped with ethanol in between the cuttings and handling was done using nitrile gloves. The segments were packed in N$_2$-flushed, vacuum sealed opaque bags and were stored at approximately 4°C (pore water analysis) or frozen (molecular analysis, lipid biomarkers, bulk analysis) before processing. Samples were frozen at −20°C on-site and were kept frozen until further processing in the lab starting in September 2019. Sampling for sediment CH_4 concentrations and isotopes as well as molecular work was done in a cleaned and weather-protected tent at the coring site without time delay after a core was retrieved. Defined sediment plugs (3 cm^3) were obtained from the edges of the 10 cm core slices using cut syringes and placed into 20 mL vials containing saturated NaCl (gas analysis) or into sterile 15 mL falcon tubes (molecular work). A total of 139 of the 10 cm segments were used for analyses: 41 from LG, 39 from LNPF, and 59 from PFL.

2.3 | Porewater sampling and analysis

Porewater samples were extracted using a hydraulic press in an anoxic glovebox and then filtered through a 0.45 μm microporous membrane. pH was measured with a WTW MultiLab 540 probe (WTW, Germany). Samples were analyzed by suppressed ion chromatography for all major cations and anions. Alkalinity was measured by colorimetric titration. Dissolved iron (ferric and ferrous) concentrations in pore water were measured via spectrophotometry by the ferrozine method (Viollier et al., 2000), with a detection limit of 0.25 μM. Samples were measured at GFZ German Research Centre for Geosciences.

2.4 | CH_4 concentrations and carbon isotopes

Concentrations of CH_4 were determined by static headspace gas chromatography (GC7890, Agilent Technologies, USA) with a flame
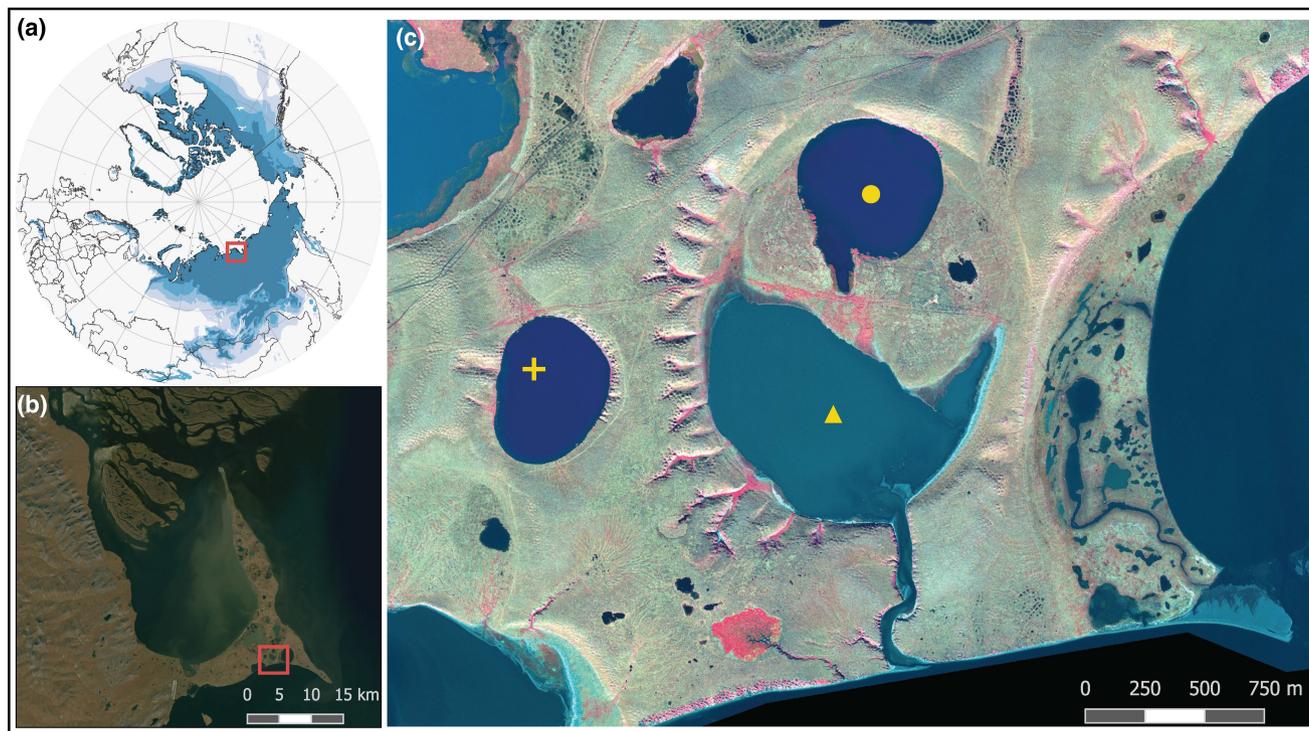
FIGURE 1 Location and map of the study site showing (a) location with respect to the Northern Hemisphere and permafrost extent regions (b) location with respect to the Bykovsky Peninsula, and (c) relative location of the lakes and the lagoon. Note the small channel at the bottom of PFL connecting to Tiksi Bay. Symbols show location of coring sites: Triangle—Polar Fox Lagoon; Circle—Northern Polar Fox Lake; Cross—Lake Golzovoye. Map in (a) based on Brown et al. (1997), (b) ESRI Satellite World Imagery, and (c) based on WorldView-3 false color satellite image (8–5–3), acquired 2016-09-02 (©DigitalGlobe). Map lines delineate study areas and do not necessarily depict accepted national boundaries.

ionizing detector (FID). Before each GC measurement, the instrument was checked against standard gasses and was newly calibrated if necessary. Plug samples were mixed into a slurry before analysis, and concentrations are presented in units of micromoles of CH_4 per gram of whole sediment plug ($\mu mol\,g^{-1}$). A sediment plug was defined as 3 cm^3 of the in-situ mixture of sediment, pore water, and pore gas. Stable carbon isotope signatures of CH_4 were analyzed by isotope-ratio mass spectrometry (Delta V plus, Thermo Scientific, Dreieich, Germany) coupled to a GC-Isolink/Trace-GC (Thermo Scientific, Dreieich, Germany) at Universität Hamburg. Values are expressed relative to Vienna Peedee belemnite (VPDB) using IAEA NGS3, (−73.3‰ VPDB) as external standards. The analytical error of these analyses was ±0.2‰.

2.5 | Bulk parameters

Samples were analyzed for total carbon (TC), total organic carbon (TOC), total nitrogen (TN), and total sulfur (TS) at the University of Cologne. For analysis of TC, TN, and TS, 20–30 mg aliquots of dry sample were combined with 20 mg of tungsten trioxide (an oxidation catalyst) and were measured on an Elementar Micro Vario elemental analyzer. For TOC measurements, samples were first processed to remove inorganic carbon by adding 1% HCl to 20–50 mg of dry bulk

sample for 1 h at 60°C, and then allowed to continue to react overnight at room temperature. Samples were then thoroughly rinsed with 18.2 MΩ purified water until pH was back to neutral values and dried in the oven at 60°C. Afterwards, 20 mg of tungsten oxide were added to each and samples were analyzed using the same Elementar Micro Vario elemental analyzer.

2.6 | Lipid biomarker indices

Lipid extraction was performed to obtain n-alkanes for use in several biomarker indices to characterize the origin of organic matter in the lakes. Samples (6–10 g dry weight) were extracted following the method of Bligh and Dyer (1959). The total lipid extracts were then separated into neutral lipid, glycolipid and phospholipid fractions using hand-packed SiOH columns and eluting with dichloromethane, acetone, and methanol, respectively. The neutral fractions (containing n-alkanes) were further separated using activated SiO_2 column chromatography and n-hexane as eluent. The n-alkanes were measured on a gas chromatograph equipped with an on-column injector and flame ionization detector (GC-FID, 5890 series II, Hewlett Packard, USA). A fused silica capillary column (Agilent DB-5MS; 50 m × 0.2 mm; film thickness: 0.33 μm) was used with helium as carrier gas. n-Alkane identification and quantification was performed

using an external standard mixture of C_{21}-C_{40} n-alkanes (PN 04071, Sigma-Aldrich).

Detailed information about the indices used can be found in the corresponding references, but briefly:

The carbon preference index (CPI) indicates the maturity of the organic matter, where higher values are generally indicative of less degraded organic matter. Crude oil, for example, has a CPI value of approximately 1. The CPI is calculated after Marzi et al. (1993):

$$CPI_{23-33} = \frac{\Sigma \text{ odd } C_{23-31} + \Sigma \text{ odd } C_{25-33}}{2 \cdot \Sigma \text{ even } C_{24-32}}.$$

The proxy P_{aq} was proposed by Ficken et al. (2000) and first applied to permafrost by Zheng et al. (2007). The P_{aq} expresses the portion of organic matter derived from submerged or floating macrophytes ($P_{aq} > 0.4$) as opposed to emergent and terrestrial plant input ($P_{aq} < 0.4$). We used the general trend of P_{aq} rather than the absolute values due to the proxy being applied to permafrost regions only recently, and not developed for this soil type

$$P_{aq} = \frac{C_{23} + C_{25}}{C_{23} + C_{25} + C_{29} + C_{31}}.$$

2.7 | DNA extraction and Illumina sequencing of amplicons and metagenomic DNA

Total nucleic acids were extracted in duplicate using the PowerSoil-Kit (MO-BIO, Qiagen) according to the manufacturer's protocol. The concentration of DNA extracts was checked via gel electrophoresis and on a Qubit fluorometer (Invitrogen).

Amplicon libraries were prepared with the barcoded primer pair Uni515-F/Uni806-R to cover both bacterial and archaeal 16S rRNA genes (Caporaso et al., 2011). Each sample was run in technical duplicate. The 50 μL PCR reactions contained 10x Pol Buffer C (Roboklon GmbH), 25 mM MgCl$_2$, 0.2 mM deoxynucleoside triphosphate (dNTP) mix (ThermoFisher Scientific), 0.5 mM each primer (TIB Molbiol, Berlin, Germany) and 1.25 U of Optitaq Polymerase (Roboklon). The PCR program started with a denaturation step at 95°C for 10 min, followed by 35 cycles at 95°C for 15 s, annealing at 60°C for 30 s, extension at 72°C for 45 s and a final extension step at 72°C for 5 min. The tagged PCR products were then purified with the Agencourt AMPure XP kit (Beckman Coulter, Switzerland) and eluted in 30 μL DNA/RNA-free water. The purified product was quantified and then the equilibrated PCR product, together with positive and negative controls, were pooled. The sequencing was performed on an Illumina MiSeq system (paired-end, 2×300 bp) by Eurofins Scientific.

In addition to amplicon sequencing, metagenomic sequencing was done on six samples of sediment from the lagoon by using the Illumina HiSeq 2500 platform by Eurofins Scientific. These six samples are representative of the sulfate zone (combination of the 40, 100, and 130 cm core segments), the upper (190 cm core segment), middle (220 cm core segment), and bottom (250 cm core segment)

of the sulfate–methane transition zone, freshwater sediment (combination of the 310, 420, and 480 cm core segments), and the talik (570 cm core segment).

2.8 | Amplicon and metagenomic data processing

For the amplicon data, raw sequences were processed according to Yang et al. (2021). The community composition was reported in ASV (amplicon sequence variants) tables using the DADA2 algorithm (Callahan et al., 2016) and the taxonomy was assigned against the SILVA138 database (https://www.arb-silva.de). In this study, special attention was paid to methanogens and aerobic/anaerobic methanotrophs. The ASV table was filtered by taxonomy to keep only methane producing archaea, and methanotrophic prokaryotes. The technical duplicates of each sample were merged. The resulting data set had 264 ASVs including methanogenic archaea, aerobic methane oxidizing bacteria (MOB) and anaerobic oxidizers of methane (AOM). A total of 23 samples (excluding technical duplicates) were analyzed: 7 each from LG and LNPF, and 9 from PFL.

Metagenomic data for the lagoon were processed including steps of quality control, assembly, and functional annotation according to the flow described by Kieser et al. (2020). Briefly, we performed quality control on Illumina data using the BBtools suite (https://sourceforge.net/projects/bbmap), and assembled with metaSpades (Nurk et al., 2017) with default settings. For the genes predicted by Prodigal (Hyatt et al., 2010), functional annotation was processed by eggNOG-mapper (v2) with DIAMOND (v0.8.22.84) (Buchfink et al., 2015) against the associated reference database eggNOG 5.0 (Cantalapiedra et al., 2021). The abundance of key functional genes (in transcripts per kilobase million, TPM) involved in methanogenesis, aerobic methane oxidation (MOB), dissimilatory nitrate reduction (DNR) and sulfate reduction (DSR) was compared to provide additional insight to the amplicon-derived data for the lagoon. To check the taxonomy bearing these genes, we taxonomically annotated the translated protein sequences of these genes using DIAMOND and compared against the UniProt90 reference database (https://www.uniprot.org).

2.9 | Network analysis

First, the ASVs with mean relative abundances of less than 0.05% across all samples were removed from downstream analysis. The resulting dataset was further filtered to only keep those ASVs with a Spearman correlation coefficient with an absolute value greater than 0.6 and a statistically significant p value of less than 0.01. These filtering steps removed poorly represented ASVs and reduced network complexity, facilitating the determination of the non-random co-occurrence of the core community. The network was then explored and visualized using the *igraph* package (v 1.2.5, Csardi & Nepusz, 2006). Community modularity was detected via a *walktrap* algorithm according to the internal ties and the pattern of ties between different groups with the *igraph* package.

To explore the association between network modularity and environment conditions, the ASV members were first used for correspondence analysis, and then the ordination object was fitted by the environmental variables with the *envfit* function in R package *vegan* (version 2.5–6) (Oksanen et al., 2019).

2.10 | Numeric and statistical analysis, and structural equation modeling

The contribution of different consortia to the total abundance and beta diversity (Bray–Curtis dissimilarity) was calculated with R package *otuSummary* (Yang, 2020). A constrained analysis, Canonical Correspondence Analysis, was used to explore the linkage between microbial community variation and environmental variables (which includes the sediment, pore water chemical composition, and CH_4 concentration and isotopic signatures) by using R package *vegan* (Oksanen et al., 2019). Variation partitioning was subsequently performed based on the returned canonical correspondence analysis object to resolve the explanatory power of pore water chemistry and sediment nutrient condition by using the *varpart* function in package *vegan*. In addition, structural equation modeling (SEM) was implemented with R package *lavaan* (v0.6.9) (Rosseel, 2012) in order to numerically estimate the observed relation between community structure and different environmental features and ecological functionality. Data visualization of environmental data, qPCR and bubble plot was performed with the *ggplot2* package (v3.3.2) (Wickham, 2016).

3 | RESULTS

3.1 | Geochemistry

The porewater and bulk geochemistry of the two freshwater lakes were very similar, though differences were seen in the CH_4 concentrations, CH_4 carbon isotopes, and iron profiles (Figure 2). While the pore water chemistry results of the lower half of the lagoon sediment were quite similar to the lakes, large differences in alkalinity, salinity, chloride and sulfate concentrations, pH, and $\delta^{13}C$-CH_4 were observed in the upper 300 cm. These results reflected the freshwater condition of the porewater of the lakes, LG and LNPF, and brackish condition pore water in the upper sediment (and surface water) of the lagoon, PFL, and demonstrated that the pore water in the deeper lagoon sediment was still in a freshwater condition. The C:N ratio was roughly similar over the entire sediment profiles of both lakes, ranging from 7–12. The C:N ratio of the upper 430 cm of sediment in the lagoon was similar to that of the lakes. However, from 430–510 cm the C:N ratio, and TOC and TN content of the lagoon were much higher than that of the lakes, and of the upper lagoon sediment.

The $\delta^{13}C$-CH_4 values in all three water bodies, except for in the sulfate-rich region of the lagoon, were highly depleted, indicating

that the most dominant production pathways were either methylotrophic or hydrogenotrophic methanogenesis. Within the sulfate-rich region of the lagoon sediments, comparatively less negative, or heavy, $\delta^{13}C$-CH_4 values indicated high rates of methane oxidation.

3.2 | Biomarker indices

The upper 200 cm of sediment of each water body generally had higher P_{aq} values than the rest of the profile, indicating that those layers were composed of more submerged and floating plants, while the deeper sediments had a larger portion of emergent macrophytes and terrestrial plants. The CPI values for both lakes and the lagoon were similar for the top 100 cm, with values between 5.5–6.5, converging again at their respective maximum core depths with CPI values of 8–9. This indicated that the organic matter in the upper sediment column was slightly more degraded (lower CPI value) than that of the deeper sediment (higher CPI value). In-between these regions the CPI was quite different for each lake indicating differences in the maturity of the organic matter and decomposition processes, or changes in the vegetation cover. For example, PFL had very degraded organic matter at approximately 350 cm compared to the less degraded organic matter at approximately 410 cm. Interestingly, the highest Fe^{2+} concentration in the pore water of PFL was also observed at this depth. This potentially signifies very reduced conditions which may be slowing degradation.

3.3 | Microbial consortia of the methane cycle

Methane cycling microbes which were derived from amplicon sequencing were separated into three main groups: methanogens, aerobic methanotrophs (methane oxidizing bacteria: MOBs), and anaerobic methanotrophs (AOMs) (Figure 3). Across all samples, methanogens were dominated by the methylotrophic Methanomassiliicoccales and Methanofastidiosales, followed by the hydrogenotrophic *Methanoregula* and obligatory acetoclastic *Methanothrix* (commonly referred to as *Methanosaeta*). *Methanosarcina* (generally acetoclastic) were scattered in some samples with relatively low abundances. This, coupled with the isotope results, indicated that methylotrophic methanogenesis is the most dominant methane production pathway.

Of the anaerobic methanotrophs, ANME-2a/2b were very abundant in the sulfate-rich sediments of the lagoon (upper 300 cm). Members of the candidate family Methylomirabilaceae, such as Sh765B-TzT-35 and Z114MB74, generally prevailed across all samples but were almost absent from the upper 300 cm of sediment of the lagoon. Other members of this same family, such as "*Candidatus* Methylomirabilis oxyfera", have been shown to couple methane oxidation to nitrite reduction (Versantvoort et al., 2018). Canonical aerobic methane oxidizers (MOBs) had very low relative abundances except for the upper 10 cm of sediment of all
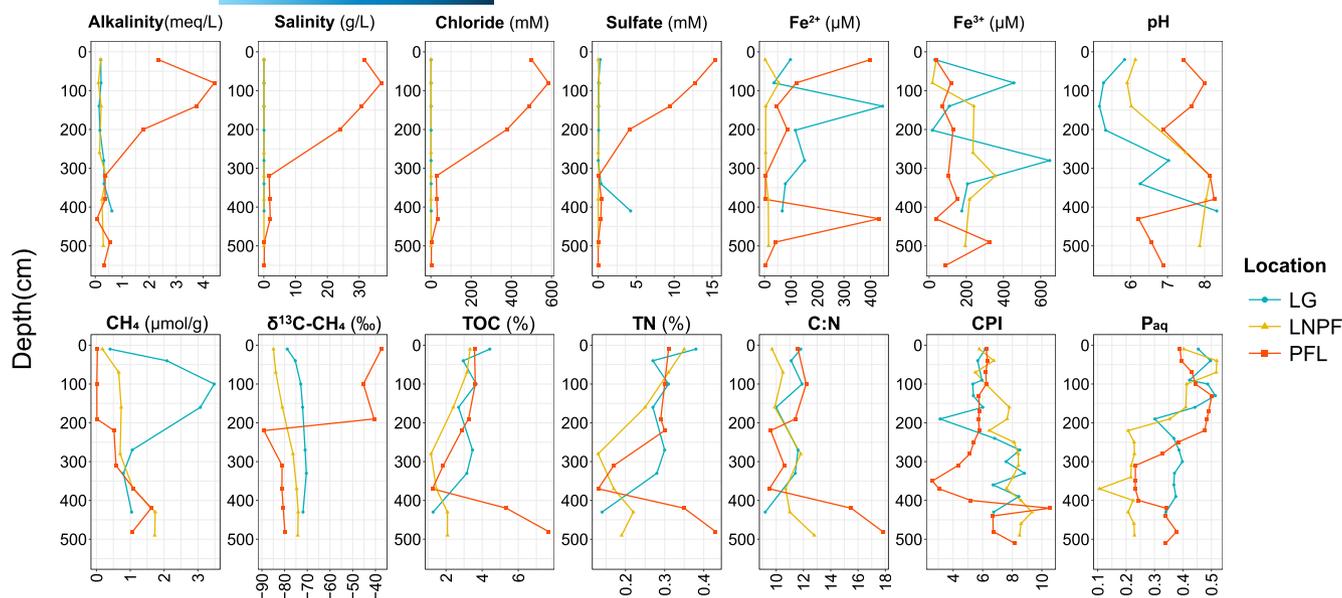
FIGURE 2 Porewater chemical features of sediments in three cores. The *y*-axis shows the depth from the sediment surface. Water height above sediment surface was 510, 560, and 310 cm for Lake Golzovoye (LG), Northern Polar Fox Lake (LNPF), and Polar Fox Lagoon (PFL), respectively. CPI, carbon preference index.

three water bodies. This indicated that aerobic methane oxidation was likely limited in the sediment column. Prevalent MOBs included mostly type I Gammaproteobacteria, such as members from *Crenothrix*, *Methylobacter*, and *Methyloprofundus* which had the highest relative abundance. Quantification of taxonomic and functional gene copy numbers through qPCR provided overall support of the relative abundances obtained from sequencing and downstream analysis. The qPCR method and results are presented in Data S1.

Metagenomic data of the lagoon sediments demonstrated a high ocurrence of genes responsible for dissimilatory sulfate reduction in the sulfate zone, and the key genes for methanogenesis (*mcrABG*) also exhibited slightly higher abundance in the sulfate zone (Figure 4). Genes which are involved in dimethylamine and trimethylamine metabolism (*mtbB* and *mttB*) were detected in the sulfate zone while the *mtmB* gene for monomethylamine metabolism was identified beneath the sulfate zone (Figure 4). The compositional variation of taxa annotated from the key genes supports this trend (Figure S1). The *pmoA* gene which is key for the canonical aerobic MOB occurred in low abundance in the two upper layers of the sulfate zone. In the sulfate zone of PFL, the *mcrABG* genes were highly associated with the taxonomic lineages of ANME-2a (ANME-2 cluster archaeon HR1, 47.4%–59.5%), followed by *Ca*. Methanoperedens (2.7%–19.3%) (Table S2). Aligned with the high occurrence of sulfate-dependent ANME2 lineage, abundant sulfate reducing genes and bacteria were also identified in the sulfate zone of the lagoon.

In the ordination space of the canonical correspondence analysis, the samples from 20–60 cm of the lagoon were generally separated from all other samples (the rest of the lagoon and the lakes) (Figure S2a). The environmental variables can explain

approximately 74% of the total inertia (i.e., community variations) in the CCA analysis. The variation partition suggested that pore water chemistry was responsible for around 44% of total variance, followed by only 11% contribution by sediment features, which included TOC, TN, C:N, CPI, and P_{aq} (Figure S2b). The SEM further highlighted the strong influence of pore water chemistry on microbial assemblages versus the influence of sediment features (Figure 5). Methanogens and MOB respectively had positive and negative influences on the concentration and isotopic signature of sediment CH_4 underlining their direct role on the fate of CH_4.

3.4 | Co-occurrence and modularity

After quality filtering, 93 ASVs were used for network construction. These ASVs on average contributed 88.75% (min: 39.38%, first quartile Q_1: 88.95%, third quartile Q_3: 96.71%, max: 99.40%) to the total abundance (which constitutes 264 ASVs) and 75.05% (Q_1: 60.44%, Q_3: 90.99%) to the total Bray–Curtis dissimilarity (BC) (Table S3). Therefore, the subset of these ASVs largely represented the populations involved in methane cycling.

The species network consisted of 93 nodes (each node representing one ASV) and 1535 undirected edges (Figure 6). The density was 0.3588, the average path length was 1.716 edges with a diameter of 3 edges, and the average clustering coefficient transitivity was 0.6848. The centrality measures (degree, betweenness, closeness and eigen centrality) highlighted the importance of the lineages belonging to Methanomassiliicocales, *Methanoregula*, Methanofastidiosales and Methylomirabilaceae in the network involved in methane cycling.
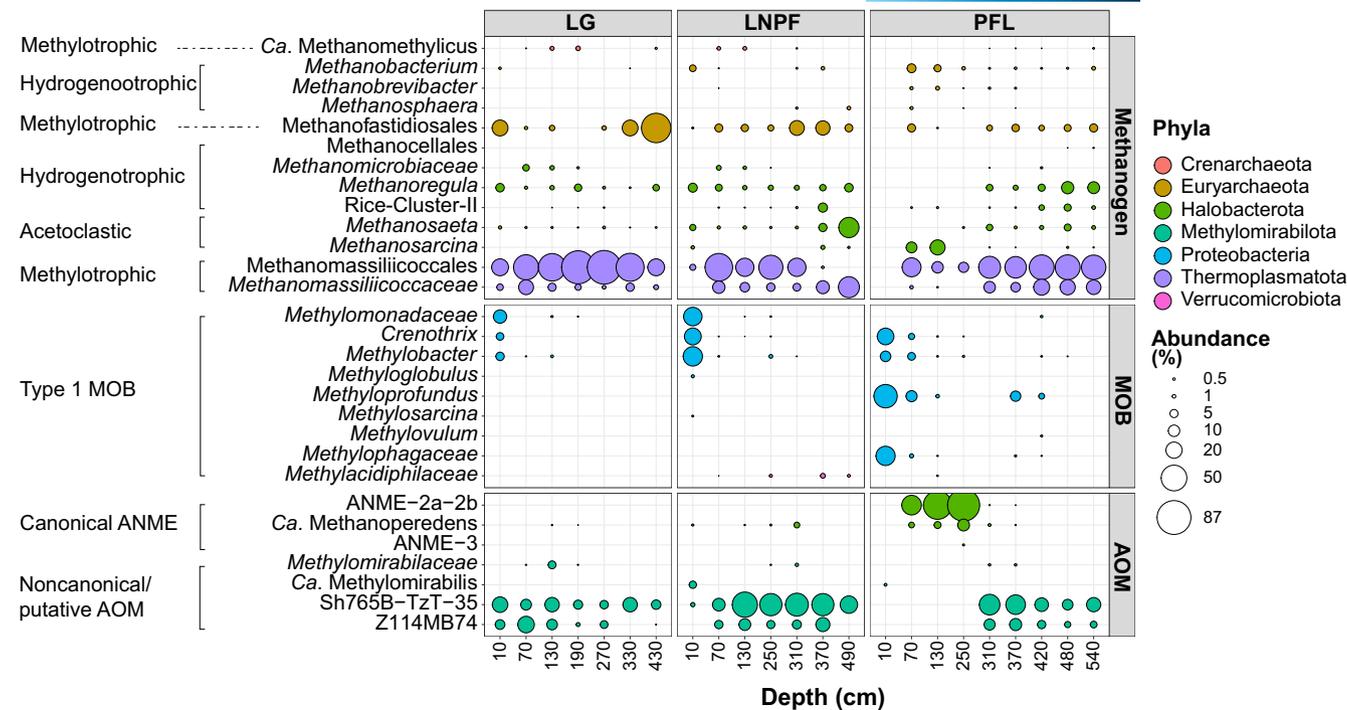
FIGURE 3 Bubble plot showing the relative abundance within the targeted subset of 264 ASVs (the abundance of all 264 ASVs sum up to 100%). The taxonomy was collapsed at genus level. If an assignment to the genus level was not possible the next higher assignable taxonomic level was used. LG: Lake Golzovoye, LNPF: Northern Polar Fox Lake, and PFL: Polar Fox Lagoon. AOM, anaerobic methane oxidizers; MOB, methane oxidizing bacteria.
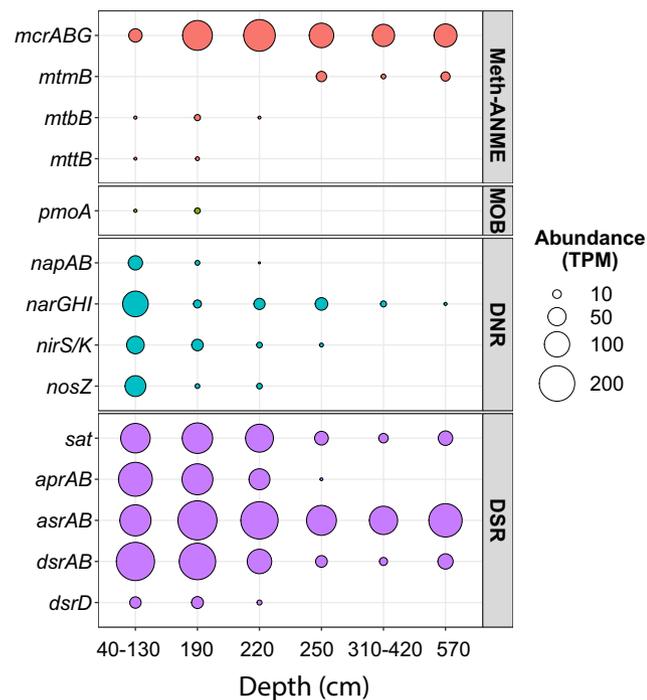

FIGURE 4 Abundance of key genes involved in methanogenesis/ANME, aerobic methane oxidization (MOB), dissimilatory nitrate reduction (DNR), and dissimilatory sulfate reduction (DSR) over six layers of Polar Fox Lagoon (PFL). The depths of 40–130 cm are in the sulfate zone; 190, 220 and 250 cm are in the upper, middle, and bottom of sulfate–methane transition zone; and depths from 310 cm and deeper are freshwater. ANME, anaerobic methanotrophic archaea.

Five modules were identified by the *walktrap* algorithm (modularity score = 0.204). With the members of each module an ordination showed that Module 1 and 4 are stretched along the first axis, suggesting association with marine-water sulfate, chloride, and alkalinity. In contrast, ASVs in Module 2, 3, and 5 are distant from the marine influenced samples, which showed stratified cluster features along axis CA2 (Figure 6; Figure S3). The distribution of different modules was likely structured by pore water chemistry. Module 2 occurred mainly in the surface samples (0–10 cm), while module 3 and 5 were distributed in down-core freshwater sediments. Across all modules, keystone taxa consisted of H_2-dependent methylotrophic methanogens which are mainly affiliated to Methanomassiliicocales or Methanofastidiosales. In Module 1 and 4, important components also include methane oxidizers like ANME-2a/b, *Candidatus* Methanoperedens and *Crenothrix*. Every module contains at least one methanogenic lineage. More specific information about which taxa were assigned to each module is available in Data S2.

4 | DISCUSSION

4.1 | Environmental conditions and history of the lagoon sediments

The porewater chemistry of the upper 300 cm of the lagoon sediments indicates that sulfate and other ions have diffused into
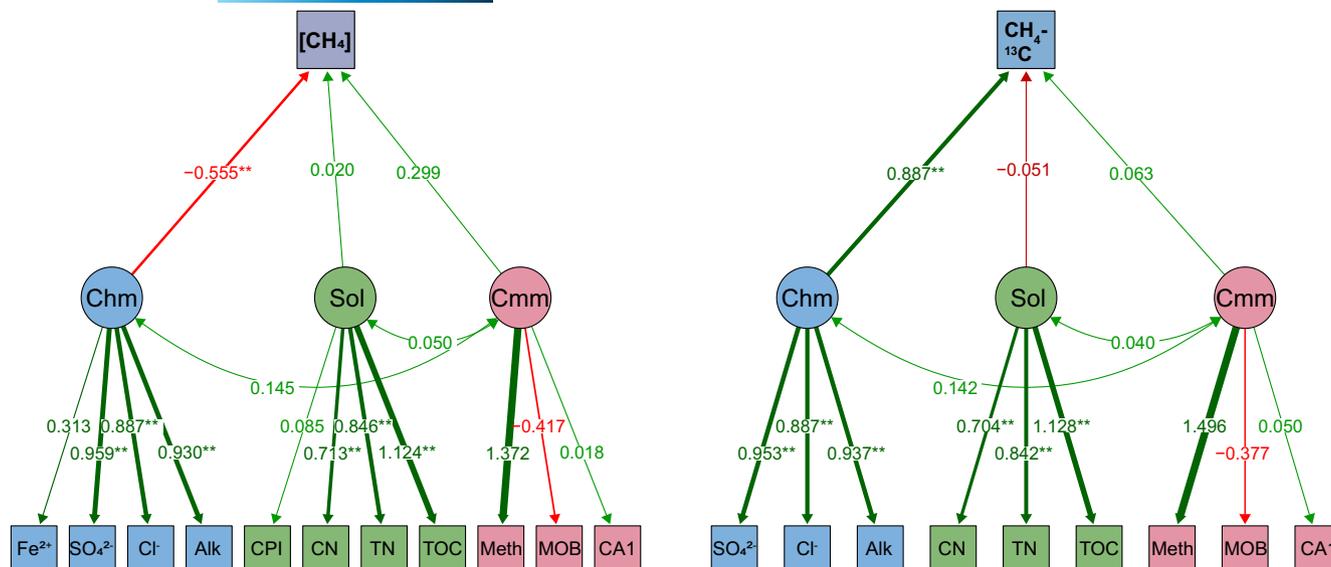
FIGURE 5 Structural equation modeling (SEM) showing the influence of latent variables, porewater chemistry (Chm), carbon and nitrogen (Sol), and Community (Cmm), on the sediment CH_4 concentration (left) and ^{13}C-CH_4 signature (right). Latent variables indicated with ovals and observed variables shown in rectangles. The residuals of observed variables is not shown here. Path coefficients standardized and significant at p-value <.05, and path width reflects the absolute value of standardized coefficients. The width of edges varies with absolute weights. Absolute weights under 0.3 become smaller in width. Edges with absolute weights under 0.01 were omitted. Meth: methanogen relative abundance, MOB: relative abundance of aerobic methane oxidizing bacteria, CA1: the first axis of corresponding analysis; Alk: alkalinity, $[CH_4]$: concentration of sediment methane ($\mu mol\,g^{-1}$). The Comparative Fit Indices (CFI) are 0.750 and 0.845 for the left and right analysis, respectively. The Root Mean Square Error of Approximation (RMSEA) are 0.234 and 0.235, respectively. The contribution of AOM had to be omitted in the SEM as the model did not converge due to many zero values of AOM over samples within the limited dataset.
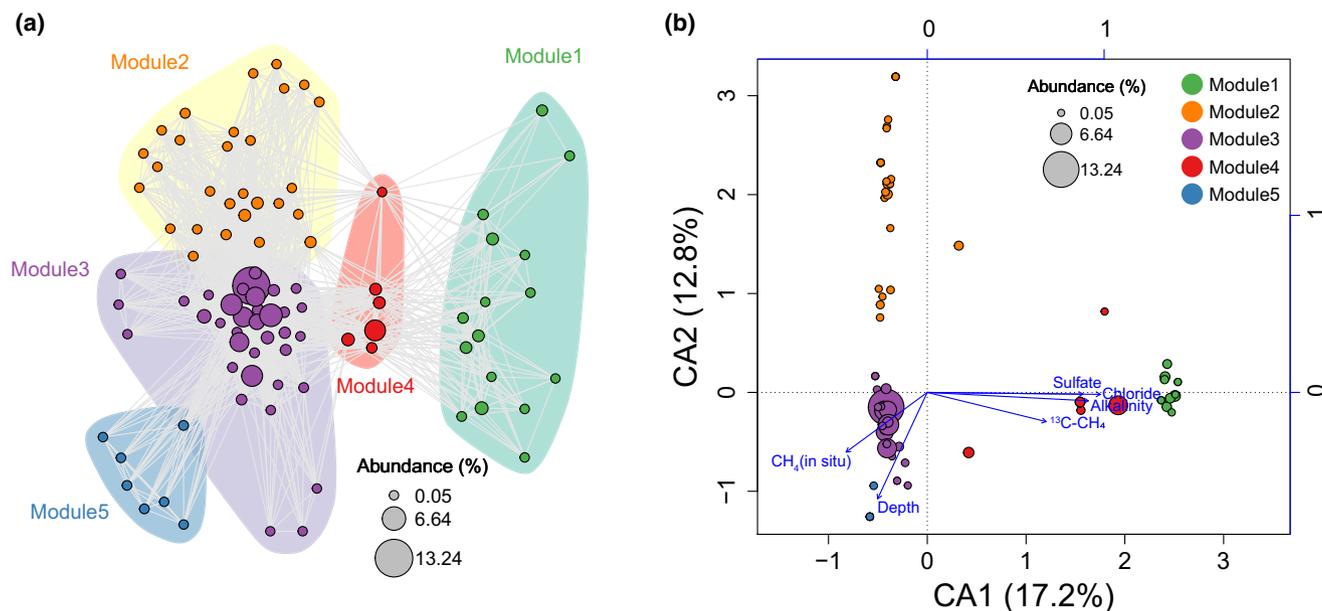

FIGURE 6 Network modules showing Modules for methane cycling consortia (a) and the association of each Module and environmental variables and features (b) in correspondence analysis ordination. Bubble size in network and ordination is corresponding to the mean relative abundance of each ASV.

sediments originally deposited under freshwater conditions, creating a marine-influenced gradient below which the porewater chemistry is comparable to the lakes. The seasonal intrusion of water from Tiksi Bay into the lagoon has fostered the formation of a sulfate zone

from approximately 0–200 cm, followed by a sulfate–methane transition zone (SMTZ) from approximately 200–400 cm. This stresses the profound effect that infiltrating water from Tiksi Bay has on the porewater chemistry of the lagoon sediment, even though the

lagoon is only connected to the bay during the ice-free summer months (Angelopoulos et al., 2020).

The trends in P_{aq} indicate that overall, organic matter was of a more terrestrial origin in deeper sediments of all studied water bodies, and has been slowly transitioning towards more submerged and floating plants in the shallower sediments. Though there are some differences in the C:N ratios, all three water bodies stay within a range of 8–18 over their entire profile, which indicates a similar, moderate, decomposition state of the organic matter within the sediments of all three lakes. This further supports that the sediment and organic matter composition of the lagoon was very similar to that of the freshwater lakes before marine water intrusion. This means that differences observed in the lagoon are more likely due to the marine water intrusion. This is also in line with the range found for a variety of permafrost deposits (5.4–72.6), as well as that found specifically in permafrost from the same region: approximately 5–30 (Walz et al., 2018). The C:N ratios could also indicate a large proportion of phytoplankton mixed into the sediments (Biskaborn et al., 2012; Vyse et al., 2020). The increase in CPI and C:N values in the range of 400–500 cm in the lagoon indicates that the organic matter there is less decomposed compared to the rest of the profile. This less degraded organic matter is possibly caused by partially refrozen sediment in the lagoon. For an explanation of coupled heat and salt flow in the sediment of this lagoon and consequences on frozen state of the sediment, see Angelopoulos et al. (2020).

4.2 | Lagoon formation promotes establishment of AOM consortia

The decrease of CH_4 concentration in the sulfate-rich upper part of the lagoon in conjunction with heavier isotopic values imply that thermokarst lagoons can establish a strong methane oxidation regime that reduces CH_4 concentrations compared to their freshwater analogs. Thermokarst lakes in the ice-rich permafrost lowland are generally hotspots of CH_4 emission (Walter et al., 2007; Walter Anthony et al., 2018), and our results from the sediment columns of the lakes, LG and LNPF, tend to agree with this given CH_4 concentrations of up to 2.21 µmol g^{-1} in LG, and up to 1.16 µmol g^{-1} in LNPF. The CH_4 present in the low sulfate sediment column of all three water bodies is likely a mixture of saturated or supersaturated porewater and small CH_4 gas bubbles. Calculations under the assumption that all measured CH_4 was dissolved in the porewater leads to concentrations of up to 17 mM in LG, much higher than the approximately 3.3–3.8 mM soluble at 1.51 bar (for 510 cm water depth) and 0–4°C in freshwater (Wiesenburg & Guinasso, 2002). In addition, ebullition was observed during sampling in the two freshwater lakes, but not in the lagoon. Bussmann et al. (2021) and Spangenberg et al. (2021) also saw extensive ebullition in LG during their sampling events. Evidence for the presence of CH_4 bubbles in the sediment or soil column have been observed in other studies, including in marine, lacustrine, and wetland environments (Pohlman et al., 2013; Thomsen et al., 2001; Tokida et al., 2005).

In comparison with the low sulfate sediment columns, the lagoon's maximum CH_4 concentration in the sulfate zone (0.02 µmol g^{-1}) was equivalent to only 0.4%–5% of the CH_4 concentrations of the rest of the lagoon sediment profile and of the concentrations along the entire profiles of both lakes. The reduction in porewater CH_4 concentration is concurrent with heavily enriched δ^{13}C-CH_4 signatures (compared to the lakes), suggesting the occurrence of substantial CH_4 oxidation. In addition, Spangenberg et al. (2021) found that the CH_4 concentration in winter ice samples of the lagoon was as low as 10% of that in Lake Golzovoye (lagoon mean: 54.7 nM vs Golzovoye mean: 645 nM), indicating that CH_4 was still effectively attenuated in winter when the lagoon is disconnected from the bay. Angelopoulos et al. (2020) found that even though the lagoon was disconnected during the winter, continued growth of the ice cover would repel ion into the liquid phase and thus caused increased salinity in the shrinking water volume during the winter months, likely preserving the marine effect.

There is evidence that methane oxidation in the lagoon is performed by canonical anaerobic methanotrophic archaea, especially the ANME-2a/2b groups. Overall, a profound shift in CH_4 cycling consortia was observed between the freshwater lakes and the sulfate-affected portion of the lagoon, corresponding to changes in geochemical composition, in particular the high sulfate concentration and salinity. In the non-sulfate-affected region of the lagoon, the microbial community is roughly the same as in the lakes at that depth. The effect of the geochemical changes was reflected in the environmental partitioning and SEM analysis. Based on the porewater chemistry, such as the Fe^{2+} concentrations, the sediments in all three profiles below the redox boundary at about 10 cm are likely anoxic (Biskaborn et al., 2013). Previous studies working on the same lakes have also found that the sediments are anoxic except for limited oxygen availability in the top few centimeters (Jenrich, 2020; Schindler, 2019; Spangenberg et al., 2021). This would generally inhibit obligate aerobic methane oxidation below this point, providing space for the anaerobic methane oxidizing community to develop, which is supported by the amplicon sequencing and metagenomic results (Figures 3 and 4) and by overall low gene copy numbers of aerobic methane oxidizers (Figure S4). Accordingly, canonical aerobic MOBs are poorly represented in these thermokarst systems, especially in the zone of PFL where CH_4 concentrations and isotopes strongly point towards methane oxidation. The metagenomic and amplicon sequencing data support the presence of multiple types of AOMs in the lagoon. The most abundant (Figure 3) are the S-AOM ANME-2a/2b which are commonly found in classical marine environments. Their dominance is also supported by high sulfate reduction rates in the sulfate zone and SMTZ of the lagoon, which was previously shown to be at least one order of magnitude higher (ca. 50–420 nM cm^{-3} day^{-1}) than the rest of the profile and the freshwater lakes. Strong sulfate reduction in the sulfate zone of PFL could also be supported by the pronounced reduction of sediment CH_4 concentration and relatively enriched δ^{13}C-CH_4 values (around −40‰) (Figure 2) and by

substantially higher gene copy numbers of sulfate reducers in the lagoon (Figure S4).

The timing of the establishment of these marine ANME consortia in the lagoon is difficult to ascertain. As previously stated, the channel opened between the lagoon and Tiksi Bay approximately 2000 years ago, giving the upper limit of the time of establishment. The lower limit is unknown, but in recent studies of marine-water inundated coastal peatlands, no S-AOMs were observed even 25 years after inundation. One example comes from Weil et al. (2020), a study which included the 'Karrendorfer Wiesen', a formerly drained peatland re-wetted with marine water in 1993, which has no established S-AOM community even more than 25 years after the rewetting. In a rewetted coastal fen near Rostock in Germany with infrequent marine water intrusion events, only archaea from the so called ANME-2d group were found which are known to use nitrate as electron acceptor, but again no sulfate-driven ANMEs (like ANME 2a/2b) were observed (Wen et al., 2018). Another study in tropical coastal lagoons by Chuang et al. (2017) found very little methane oxidation activity even though sulfate and CH_4 concentrations were high.

Nitrate is also a viable terminal electron acceptor for AOM. Nitrate concentrations in the porewater, although very low in all three profiles, agree with nitrate concentrations in natural environments, which rarely exceed 50 μM (Schink, 2010). Porewater nitrate concentrations of the lagoon being below the detection limit may be a consequence of fast nitrate reduction, rather than a lack of nitrate production. This is supported the by high abundances of genes associated with denitrification and through occurrence of *Candidatus* Methanoperedens, known to couple AOM with nitrate reduction.

Ferric iron (Fe^{3+}), which is present in the low sulfate sediments of the lagoon, has also been highlighted as a potential alternative electron acceptor for methane oxidation in many other anoxic habitats (Ettwig et al., 2016; Rooze et al., 2016; Winkel et al., 2018). Such a pathway, according to a recent analysis on eutrophic coastal areas, can play an important role in mitigating CH_4 by coupling its oxidation with iron, manganese, or nitrate reduction beyond the sulfate zone in anoxic sediments due to eutrophication-associated hypoxia (Wallenius et al., 2021). Indeed, Hultman et al. (2015) found relatively high rates of iron reduction in permafrost and active zone soil incubations, indicating that iron reduction is an important process in permafrost areas. However, iron cycling is also intricately tied to methane release during thaw, with iron reduction processes causing increased emissions of methane in a thawing Palsa environment (Patzner et al., 2022). Thus, in order to fully understand the role iron plays in these environments, more targeted research is needed.

In addition to the results presented here, the work by Schindler (2019) utilizing ^{14}C-CH_4 labelling experiments also found clear evidence of AOM in the 0–200 cm lagoon sediments. Samples used by Schindler (2019) were from the cores as those used in this study. It is interesting that within the deeper sediments of LNPF and PFL, small pockets of known aerobic MOBs are present and seemingly coexisting with canonical AOM and methanogenic organisms, indicating that while this habitat is certainly not ideal for aerobic methanotrophs, it is also not completely inhospitable. As we did

not perform any transcriptome analyses, we cannot make any inferences on the metabolic state of any specific group of methane oxidizers. Recent studies of other systems found evidence of methane oxidation in anaerobic sediment performed by lineages of canonical aerobic methanotrophs (MOB). For example, in their study of sub-Arctic lake sediments Martinez-Cruz et al. (2017) found that after a six-month incubation under anoxic conditions supporting methane oxidation, type I methanotrophs from the *Methylobacter* genus were the major driver of methane oxidation. This was similar to the findings of Su et al. (2015) in the anoxic sediments of a lake in Switzerland, where type I and type II aerobic methanotrophs were found to grow under both oxic and anoxic incubation conditions. In the lakes and lagoon, *Methylobacter*, and other type I methanotrophs are present, however they are most abundant in the top 10–20 cm of sediment and for the most part represent less than 1% of total abundance (Figure 3). *Crenothrix*, a known aerobic MOB, which could survive under slightly oxygen-deficient conditions in stratified lakes (Oswald et al., 2017), is also concentrated only within the top 10 cm of both lakes and the lagoon similar to other canonical MOB (Figure 3). Thus, while these organisms may be contributing to the total AOM process in sediments of all three water bodies, their contribution must be considered marginal relative to that of methanotrophic archaea (ANMEs) in the lagoon.

The abundant occurrence of the unclassified environmental groups Sh765B-TzT-35 and Z114MB74 (Figure 3) closely related with *Candidatus* Methylomirabilales, another known methane oxidizer (Ettwig et al., 2010), imply their ecological importance. The available genomes of Methylomirabilales demonstrated the existence of genes encoding particulate methane monooxygenase (pMMO) (Versantvoort et al., 2018). A recent stable isotope probing (SIP) study in wet forest soil showed that members of Sh765B-TzT-35 act as active anaerobic methanotrophs along with methylotrophic methanogens of *Methanomassiliicoccus*, which were proposed as positive biological indicators of methanotrophy and methanogenesis in wet forest soils (Nakamura, 2019). However, our understanding of the role of these clades is extremely poor and it remains open if Sh765B-TzT-35 and Z114MB74 members contribute to methane oxidation in the sediments of this study.

4.3 | Methylotrophic methanogens and the implications of their dominance

The methanogenic consortia were dominated by methylotrophic lineages, and their prevalence across all modules and depths (Figure 3) underscores the ecological importance of methylotrophic methanogenesis in all three water bodies. Methylotrophic methanogenesis has long been considered the least utilized methanogenesis pathway, with many studies instead focusing on hydrogenotrophic and acetoclastic methanogenesis. As Zalman et al. (2018) states, this thinking is so prevalent that rates of acetoclastic methanogenesis from mixed microbial communities have been determined by subtracting the rate of hydrogenotrophic methanogenesis from the

total CH_4 production rate. This method is particularly problematic as methylotrophic methanogens do not appear to be affected by one of the most commonly used acetoclastic methanogenesis inhibitors, methyl fluoride (Penger et al., 2012). As described by Kurth et al. (2020) and Sollinger and Urich (2019), there are a wealth of substrates that various methylotrophic methanogens can and do utilize, many of which are non-competitive. Recent studies have also found that methylotrophic methanogenesis may be the dominant pathway in multiple environments. For example, Xiao et al. (2018) found methylotrophic methanogenesis to be the dominant CH_4 production pathway in sulfate-rich marine surface sediments from Aarhus Bay in Denmark. Zalman et al. (2018) found that Northern Minnesota peat bogs have a strong potential for methylotrophic methanogenesis based on the amounts of methylated substrate found there. Feldewert et al. (2020) suggested that methylotrophic methanogens are even able to outcompete hydrogenotrophic methanogens for H_2 when their habitats can provide sufficient methyl groups, even in the presence of sulfate. This study can now be added to the growing list of environments, both freshwater and marine, where methylotrophic methanogenesis is either found to be dominant, or found to have strong potential.

4.4 | Lagoon environments are unique from marine environments

The lagoon forms a microbial habitat unique not only from the freshwater sediments but also from marine sediments. In marine environments, ANME consortia are typically restricted to a SMTZ (Beulig et al., 2019; Egger et al., 2018; Nauhaus et al., 2002), whereas in the lagoon their abundance remains high in the sulfate zone above the observed SMTZ (Figure 3; Table S2). This could indicate that the location of the SMTZ in the lagoon is seasonally more variable than in marine sediments due to the dynamic nature of the lagoon (e.g., ice buildup and retreat, alternation between freshwater and brackish water inflow) but the reason for the spatially more spread ANME consortia in the lagoon in comparison with marine sediments would require further, more temporally resolved studies.

The observed prevalence of methanogens throughout the sulfate zone and SMTZ would have been a surprising finding under the classical understanding that sulfate reducers outcompete methanogens in high sulfate environments (e.g., Claypool and Kaplan (1974); Sansone and Martens (1981)). However, recent studies have also found co-habitation of methanogenesis and sulfate reduction in a few marine environments (Ozuolmez et al., 2015, 2020; Sela-Adler et al., 2017), as well as coastal marine sediments (Koebsch et al., 2019; Rooze et al., 2016). This finding is still an important distinction between classical marine environments and a lagoon environment. Mitterer (2010) proposed that the co-occurrence of methanogenesis and sulfate reduction is supported by the presence and utilization of non-competitive methanogenic substrates, such as methylamines and methylated sulfur compounds. Another

potential explanation of these differences is the intrusion of freshwater in the lagoon and coastal marine environment. Compared with a lagoon system, marine sediments in the open ocean generally contain a higher sulfate content, while the organic matter is more diluted. It is therefore conceivable that marine sediment, aside from coastal regions, also has a reduced amount of available labile carbon. Previous paleoclimate reconstructions have shown that the sediments of the lakes and lagoons on the peninsula are mixtures of permafrost thawed in situ under the waterbody, permafrost eroded from shores by thermo-erosion, and lacustrine sedimentation that has accumulated over approximately 8000 years (Jongejans et al., 2020). The carbon densities in lagoons in Yedoma permafrost regions are on average 16.5 $kg m^{-3}$, which falls within the range of terrestrial Yedoma (8 $kg m^{-3}$) and thermokarst (24 $kg m^{-3}$) sediments in the Yedoma region (Jenrich, 2020; Vyse et al., 2021). The upper three to five meters of sediment contain a higher density of carbon than those below. Moreover, the organic carbon in thermokarst lagoons is strongly correlated with the origin of the organic matter and the depositional conditions (Jenrich et al., 2021; Jongejans et al., 2020). The quality of organic carbon is an important variable regulating microbial carbon turnover (Schuur et al., 2015; Wagner et al., 2005). Likely, thermokarst lakes and lagoons can provide sufficient labile organic carbon for microbial metabolism, in excess of what is usually available in marine environments, and which is another key precondition for the coexistence of sulfate reducing bacteria (SRB) and methanogens (Ozuolmez et al., 2015; Sela-Adler et al., 2017). Therefore, the lagoon provides a sulfate and carbon rich habitat distinctly different from generally carbon poor classical non-coastal marine systems, and based on the prevalence of non-competitive methylotrophic methanogens, may also contain a larger range of organic carbon compounds.

5 | CONCLUSION AND PERSPECTIVES

In Arctic coastal permafrost regions, the transition from thermokarst lakes to lagoons changes the ionic strength and oxidative capacity, and introduces new microbial species. Consequently, the initial geochemical and trophic stratification is reorganized which in turn induces profound shifts in the structure and functionality of the methane-cycling community, and influences carbon feedbacks in the lagoon by supporting a strong AOM community. The results of our study also indicate that, while considerably different from classical marine environments, lagoon environments can still be favorable habitats for canonical AOM consortia. In the lagoon system, a high load of organic carbon and non-competitive substrates further afford the co-existence of methanogens and other sulfate-reducing organisms. They are also an acceptable habitat for the establishment of new microbial communities (Module 1, Figure 7), and mixed communities (Module 4, Figure 7). Our study also shows that the original microbial community present before lagoon development persists under the new conditions (Modules
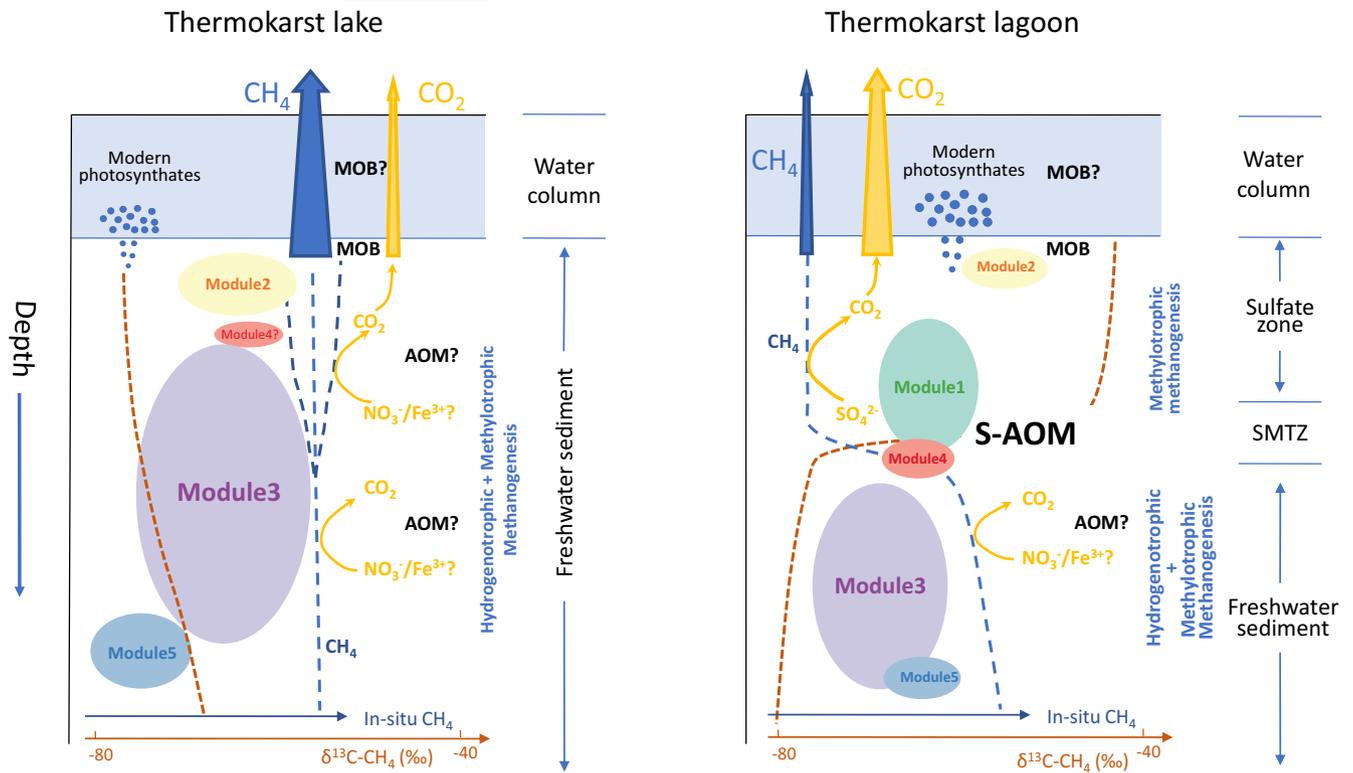
FIGURE 7 Schematic plot showing the stratified distribution of methane-cycling communities and processes in freshwater thermokarst lakes (left), and re-assembly of community and methane turnover pathways after thermokarst lakes turn into thermokarst lagoons (right). All Modules contain H_2-dependent methylotrophic methanogens. Module 1 is only found in the sulfate-zone of the lagoon, and is comprised of microbes preferring more marine conditions, especially marine AOMs. Module 4 has a smaller selection of AOM microbes, including one ASV of marine origin which is only found in the lagoon but is associated with the other microbes in the Module found also in the lakes. Modules 2, 3, and 5 are seen in both the lakes and lagoon and consist of varying types of methanogens, MOBs, and terrestrial-origin AOMs.

2, 3, and 5; Figure 7). Owing to effective methane oxidation, thermokarst lagoons mitigate sediment methane concentrations compared to freshwater thermokarst ecosystems. However, the impact of these local mitigations on the global permafrost methane flux is unknown.

An estimation of the current extent of pan-Arctic lagoons including lagoons along the coasts of the Laptev, East Siberia, Chuckhi, and Beaufort shelf seas, shows that these lagoons currently occupy an area of $2579\,km^2$ (Jenrich et al., 2022), which is roughly equivalent to the size of the country of Luxemburg. Although still comparatively small in area, thermokarst lagoons transform microbial methane cycling communities and will further expand in Arctic regions, especially along the Laptev Sea coast due to sea-level rise, accelerated permafrost thaw, intensified coastal erosion, and changing sea ice regimes. Pan-arctic lagoons may therefore be more relevant to the present-day and future permafrost carbon budget than is currently reflected in the literature, especially if they host a strong AOM community like shown here. Beyond that, thermokarst lagoon systems represent important natural laboratories for studying the effect of sea level rise on vulnerable, organic-rich coastal permafrost landscapes. Therefore, their potential to serve as habitat for efficient AOM-communities deserves more attention in the future.

from AWI and GFZ as well as the ERC PETA-CARB project. Open Access funding enabled and organized by Projekt DEAL.

CONFLICT OF INTEREST STATEMENT

The authors have no conflicts of interest.

DATA AVAILABILITY STATEMENT

The data that support the findings of this study are openly available from two different repositories. Sequencing data and metadata were deposited in the European Nucleotide Archive (ENA) at https://www.ebi.ac.uk/ena/browser/view/PRJEB49195, reference number PRJEB49195 (Yang et al., 2022a). The sample accession numbers are listed in Table S1. The metagenomic data were deposited in the ENA at https://www.ebi.ac.uk/ena/browser/view/PRJNA821074, reference number PRJNA821074 (Berben et al., 2022). The geochemistry data were deposited in the GFZ Data Services' Geoscience Data Publisher at http://doi.org/10.5880/GFZ.3.7.2022.001, reference number GFZ.3.7.2022.001 (Yang et al., 2022b).

ORCID

Sizhong Yang https://orcid.org/0000-0001-8417-593X
Sara E. Anthony https://orcid.org/0000-0002-7945-4480
Maren Jenrich https://orcid.org/0000-0002-1330-7461
Michiel H. in 't Zandt https://orcid.org/0000-0002-0497-4502
Jens Strauss https://orcid.org/0000-0003-4678-4982
Pier Paul Overduin https://orcid.org/0000-0001-9849-4712
Guido Grosse https://orcid.org/0000-0001-5895-2141
Michael Angelopoulos https://orcid.org/0000-0003-2574-5108
Boris K. Biskaborn https://orcid.org/0000-0003-2378-0348
Mikhail N. Grigoriev https://orcid.org/0000-0003-1997-9506
Dirk Wagner https://orcid.org/0000-0001-5064-497X
Christian Knoblauch https://orcid.org/0000-0002-7147-1008
Andrea Jaeschke https://orcid.org/0000-0003-2518-2739
Janet Rethemeyer https://orcid.org/0000-0001-6698-4186
Jens Kallmeyer https://orcid.org/0000-0002-6440-1140
Susanne Liebner https://orcid.org/0000-0002-9389-7093

REFERENCES

Anders, K., Marx, S., Boike, J., Herfort, B., Wilcox, E. J., Langer, M., Marsh, P., & Höfle, B. (2020). Multitemporal terrestrial laser scanning point clouds for thaw subsidence observation at Arctic permafrost monitoring sites. *Earth Surface Processes and Landforms*, *45*(7), 1589–1600. https://doi.org/10.1002/esp.4833

Angelopoulos, M., Overduin, P. P., Jenrich, M., Nitze, I., Günther, F., Strauss, J., Westermann, S., Schirrmeister, L., Kholodov, A., Krautblatter, M., Grigoriev, M. N., & Grosse, G. (2021). Onshore thermokarst primes subsea permafrost degradation. *Geophysical Research Letters*, *48*(20), e2021GL093881. https://doi.org/10.1029/2021gl093881

Angelopoulos, M., Overduin, P. P., Westermann, S., Tronicke, J., Strauss, J., Schirrmeister, L., Biskaborn, B. K., Liebner, S., Maksimov, G., Grigoriev, M. N., & Grosse, G. (2020). Thermokarst Lake to lagoon transitions in eastern Siberia: Do submerged Taliks refreeze? *Journal of Geophysical Research: Earth Surface*, *125*(10), e2019JF005424. https://doi.org/10.1029/2019jf005424

Antonova, S., Sudhaus, H., Strozzi, T., Zwieback, S., Kääb, A., Heim, B., Langer, M., Bornemann, N., & Boike, J. (2018). Thaw subsidence

of a Yedoma landscape in northern Siberia, measured in situ and estimated from TerraSAR-X interferometry. *Remote Sensing*, *10*(4), 494.

Berben, T., Forlano Bó, F., In 't Zandt, M. H., Yang, S., Liebner, S., & Welte, C. U. (2022). *Metagenomic sequencing of sediment of the polar fox lagoon*. Bykovsky Peninsula, Siberia, Russia https://www.ebi.ac.uk/ena/browser/view/PRJNA821074

Beulig, F., Roy, H., McGlynn, S. E., & Jorgensen, B. B. (2019). Cryptic CH_4 cycling in the sulfate-methane transition of marine sediments apparently mediated by ANME-1 archaea. *The ISME Journal*, *13*(2), 250–262. https://doi.org/10.1038/s41396-018-0273-z

Biskaborn, B. K., Herzschuh, U., Bolshiyanov, D., Savelieva, L., Zibulski, R., & Diekmann, B. (2012). Late Holocene thermokarst variability inferred from diatoms in a lake sediment record from the Lena Delta, Siberian Arctic. *Journal of Paleolimnology*, *49*(2), 155–170. https://doi.org/10.1007/s10933-012-9650-1

Biskaborn, B. K., Herzschuh, U., Bolshiyanov, D. Y., Schwamborn, G., & Diekmann, B. (2013). Thermokarst processes and depositional events in a Tundra Lake, Northeastern Siberia. *Permafrost and Periglacial Processes*, *24*(3), 160–174. https://doi.org/10.1002/ppp.1769

Biskaborn, B. K., Smith, S. L., Noetzli, J., Matthes, H., Vieira, G., Streletskiy, D. A., Schoeneich, P., Romanovsky, V. E., Lewkowicz, A. G., Abramov, A., Allard, M., Boike, J., Cable, W. L., Christiansen, H. H., Delaloye, R., Diekmann, B., Drozdov, D., Etzelmuller, B., Grosse, G., ... Lantuit, H. (2019). Permafrost is warming at a global scale. *Nature Communications*, *10*(1), 264. https://doi.org/10.1038/s41467-018-08240-4

Bligh, E. G., & Dyer, W. J. (1959). A rapid method of total lipid extraction and purification. *Canadian Journal of Biochemisty and Physiology*, *37*(8), 911–917. https://doi.org/10.1139/o59-099

Bouchard, F., MacDonald, L. A., Turner, K. W., Thienpont, J. R., Medeiros, A. S., Biskaborn, B. K., Korosi, J., Hall, R. I., Pienitz, R., & Wolfe, B. B. (2016). Paleolimnology of thermokarst lakes: A window into permafrost landscape evolution. *Arctic Science*, *3*(2), 91–117.

Brown, J., Ferrians, O. J., Jr., Heginbottom, J. A., & Melnikov, E. S. (1997). *Circum-Arctic map of permafrost and ground-ice conditions*. Circum-Pacific Map 45. http://pubs.er.usgs.gov/publication/cp45

Buchfink, B., Xie, C., & Huson, D. H. (2015). Fast and sensitive protein alignment using DIAMOND. *Nature Methods*, *12*(1), 59–60. https://doi.org/10.1038/nmeth.3176

Bussmann, I., Fedorova, I., Juhls, B., Overduin, P. P., & Winkel, M. (2021). Methane dynamics in three different Siberian water bodies under winter and summer conditions. *Biogeosciences*, *18*(6), 2047–2061. https://doi.org/10.5194/bg-18-2047-2021

Callahan, B. J., McMurdie, P. J., Rosen, M. J., Han, A. W., Johnson, A. J., & Holmes, S. P. (2016). DADA2: High-resolution sample inference from illumina amplicon data. *Nature Methods*, *13*(7), 581–583. https://doi.org/10.1038/nmeth.3869

Cantalapiedra, C. P., Hernandez-Plaza, A., Letunic, I., Bork, P., & Huerta-Cepas, J. (2021). eggNOG-mapper v2: Functional annotation, orthology assignments, and domain prediction at the metagenomic scale. *Molecular Biology and Evolution*, *38*(12), 5825–5829. https://doi.org/10.1093/molbev/msab293

Caporaso, J. G., Lauber, C. L., Walters, W. A., Berg-Lyons, D., Lozupone, C. A., Turnbaugh, P. J., Fierer, N., & Knight, R. (2011). Global patterns of 16S rRNA diversity at a depth of millions of sequences per sample. *Proceedings of the National Academy of Sciences of the United States of America*, *108*(Suppl 1), 4516–4522. https://doi.org/10.1073/pnas.1000080107

Chuang, P. C., Young, M. B., Dale, A. W., Miller, L. G., Herrera-Silveira, J. A., & Paytan, A. (2017). Methane fluxes from tropical coastal lagoons surrounded by mangroves, Yucatán, Mexico. *Journal of Geophysical Research: Biogeosciences*, *122*(5), 1156–1174. https://doi.org/10.1002/2017jg003761

Claypool, G. E., & Kaplan, I. (1974). The origin and distribution of methane in marine sediments. In *Natural gases in marine sediments* (pp. 99–139). Springer.

Csardi, G., & Nepusz, T. (2006). The igraph software package for complex network research. *InterJournal, Complex Systems*, 1695(5), 1–9. http://igraph.org

Dean, J. F., Middelburg, J. J., Röckmann, T., Aerts, R., Blauw, L. G., Egger, M., Jetten, M. S. M., de Jong, A. E. E., Meisel, O. H., Rasigraf, O., Slomp, C. P., In 't Zandt, M. H., & Dolman, A. J. (2018). Methane feedbacks to the global climate system in a warmer world. *Reviews of Geophysics*, 56(1), 207–250. https://doi.org/10.1002/2017rg000559

Egger, M., Riedinger, N., Mogollón, J. M., & Jørgensen, B. B. (2018). Global diffusive fluxes of methane in marine sediments. *Nature Geoscience*, 11(6), 421–425. https://doi.org/10.1038/s41561-018-0122-8

Ernakovich, J. G., Barbato, R. A., Rich, V. I., Schadel, C., Hewitt, R. E., Doherty, S. J., Whalen, E. D., Abbott, B. W., Barta, J., Biasi, C., Chabot, C. L., Hultman, J., Knoblauch, C., Vetter, M., Leewis, M. C., Liebner, S., Mackelprang, R., Onstott, T. C., Richter, A., ... Winkel, M. (2022). Microbiome assembly in thawing permafrost and its feedbacks to climate. *Global Change Biology*, 28, 5007–5026. https://doi.org/10.1111/gcb.16231

Ettwig, K. F., Butler, M. K., Le Paslier, D., Pelletier, E., Mangenot, S., Kuypers, M. M., Schreiber, F., Dutilh, B. E., Zedelius, J., de Beer, D., Gloerich, J., Wessels, H. J., van Alen, T., Luesken, F., Wu, M. L., van de Pas-Schoonen, K. T., Op den Camp, H. J., Janssen-Megens, E. M., Francoijs, K. J., ... Strous, M. (2010). Nitrite-driven anaerobic methane oxidation by oxygenic bacteria. *Nature*, 464(7288), 543–548. https://doi.org/10.1038/nature08883

Ettwig, K. F., Zhu, B., Speth, D., Keltjens, J. T., Jetten, M. S. M., & Kartal, B. (2016). Archaea catalyze iron-dependent anaerobic oxidation of methane. *Proceedings of the National Academy of Sciences of the United States of America*, 113(45), 12792–12796. https://doi.org/10.1073/pnas.1609534113

Feldewert, C., Lang, K., & Brune, A. (2020). The hydrogen threshold of obligately methyl-reducing methanogens. *FEMS Microbiology Letters*, 367(17), fnaa137. https://doi.org/10.1093/femsle/fnaa137

Ficken, K. J., Li, B., Swain, D. L., & Eglinton, G. (2000). An n-alkane proxy for the sedimentary input of submerged/floating freshwater aquatic macrophytes. *Organic Geochemistry*, 31(7–8), 745–749. https://doi.org/10.1016/s0146-6380(00)00081-4

Froelich, P. N., Klinkhammer, G. P., Bender, M. L., Luedtke, N. A., Heath, G. R., Cullen, D., Dauphin, P., Hammond, D., Hartman, B., & Maynard, V. (1979). Early oxidation of organic matter in pelagic sediments of the eastern equatorial Atlantic: Suboxic diagenesis. *Geochimica et Cosmochimica Acta*, 43(7), 1075–1090. https://doi.org/10.1016/0016-7037(79)90095-4

Grosse, G., Schirrmeister, L., Siegert, C., Kunitsky, V. V., Slagoda, E. A., Andreev, A. A., & Dereviagyn, A. Y. (2007). Geological and geomorphological evolution of a sedimentary periglacial landscape in Northeast Siberia during the Late Quaternary. *Geomorphology*, 86(1–2), 25–51. https://doi.org/10.1016/j.geomorph.2006.08.005

Hinrichs, K. U., & Boetius, A. (2002). The anaerobic oxidation of methane: New insights in microbial ecology and biogeochemistry. In G. Wefer, D. Billett, D. Hebbeln, B. B. Jørgensen, M. Schlüter, & T. C. E. van Weering (Eds.), *Ocean margin systems* (pp. 457–477). Springer.

Hinrichs, K. U., Hayes, J. M., Sylva, S. P., Brewer, P. G., & DeLong, E. F. (1999). Methane-consuming archaebacteria in marine sediments. *Nature*, 398(6730), 802–805. https://doi.org/10.1038/19751

Hugelius, G., Strauss, J., Zubrzycki, S., Harden, J. W., Schuur, E. A. G., Ping, C. L., Schirrmeister, L., Grosse, G., Michaelson, G. J., Koven, C. D., O'Donnell, J. A., Elberling, B., Mishra, U., Camill, P., Yu, Z., Palmtag, J., & Kuhry, P. (2014). Estimated stocks of circumpolar permafrost carbon with quantified uncertainty ranges and identified data gaps. *Biogeosciences*, 11(23), 6573–6593. https://doi.org/10.5194/bg-11-6573-2014

Hultman, J., Waldrop, M. P., Mackelprang, R., David, M. M., McFarland, J., Blazewicz, S. J., Harden, J., Turetsky, M. R., McGuire, A. D., Shah, M. B., VerBerkmoes, N. C., Lee, L. H., Mavrommatis, K., & Jansson, J. K. (2015). Multi-omics of permafrost, active layer and thermokarst bog soil microbiomes. *Nature*, 521(7551), 208–212. https://doi.org/10.1038/nature14238

Hyatt, D., Chen, G. L., Locascio, P. F., Land, M. L., Larimer, F. W., & Hauser, L. J. (2010). Prodigal: Prokaryotic gene recognition and translation initiation site identification. *BMC Bioinformatics*, 11(1), 119. https://doi.org/10.1186/1471-2105-11-119

In 't Zandt, M. H., Liebner, S., & Welte, C. U. (2020). Roles of thermokarst lakes in a warming world. *Trends in Microbiology*, 28(9), 769–779. https://doi.org/10.1016/j.tim.2020.04.002

Jenrich, M. (2020). *Thermokarst lagoons—carbon pools and panarctic distribution*. University of Potsdam, Potsdam, Germany.

Jenrich, M., Angelopoulos, M., Grosse, G., Overduin, P. P., Schirrmeister, L., Nitze, I., Biskaborn, B. K., Liebner, S., Grigoriev, M., Murray, A., Jongejans, L. L., & Strauss, J. (2021). Thermokarst lagoons: A core-based assessment of depositional characteristics and an estimate of carbon pools on the Bykovsky Peninsula. *Frontiers in Earth Science*, 9, 637899. https://doi.org/10.3389/feart.2021.637899

Jenrich, M., Nitze, I., Laboor, S., Angelopoulos, M., Grosse, G., & Strauss, J. (2022). *Spatial extent of thermokarst lagoons along pan-Arctic coasts—an upscaling approach*. https://doi.org/10.1594/PANGAEA.948267

Jongejans, L. L., Mangelsdorf, K., Schirrmeister, L., Grigoriev, M. N., Maksimov, G. M., Biskaborn, B. K., Grosse, G., & Strauss, J. (2020). n-Alkane characteristics of thawed permafrost deposits below a thermokarst lake on Bykovsky Peninsula, Northeastern Siberia. *Frontiers in Environmental Science*, 8, 118. https://doi.org/10.3389/fenvs.2020.00118

Jørgensen, B. B. (2006). Bacteria and marine biogeochemistry. In H. D. Schulz & M. Zabel (Eds.), *Marine Geochemistry* (pp. 169–206). Springer Berlin Heidelberg. https://doi.org/10.1007/3-540-32144-6_5

Kieser, S., Brown, J., Zdobnov, E. M., Trajkovski, M., & McCue, L. A. (2020). ATLAS: A Snakemake workflow for assembly, annotation, and genomic binning of metagenome sequence data. *BMC Bioinformatics*, 21(1), 257. https://doi.org/10.1186/s12859-020-03585-4

Knittel, K., & Boetius, A. (2009). Anaerobic oxidation of methane: Progress with an unknown process. *Annual Review of Microbiology*, 63(1), 311–334. https://doi.org/10.1146/annurev.micro.61.080706.093130

Knittel, K., Losekann, T., Boetius, A., Kort, R., & Amann, R. (2005). Diversity and distribution of methanotrophic archaea at cold seeps. *Applied and Environmental Microbiology*, 71(1), 467–479. https://doi.org/10.1128/AEM.71.1.467-479.2005

Knittel, K., Wegener, G., & Boetius, A. (2019). Anaerobic methane oxidizers. In T. J. McGenity (Ed.), *Microbial communities utilizing hydrocarbons and lipids: Members, metagenomics and ecophysiology* (pp. 113–132). Springer International Publishing. https://doi.org/10.1007/978-3-030-14785-3_7

Koebsch, F., Winkel, M., Liebner, S., Liu, B., Westphal, J., Schmiedinger, I., Spitzy, A., Gehre, M., Jurasinski, G., & Köhler, S. (2019). Sulfate deprivation triggers high methane production in a disturbed and rewetted coastal peatland. *Biogeosciences*, 16(9), 1937–1953.

Kurth, J. M., Op den Camp, H. J. M., & Welte, C. U. (2020). Several ways one goal-methanogenesis from unconventional substrates. *Applied Microbiology and Biotechnology*, 104(16), 6839–6854. https://doi.org/10.1007/s00253-020-10724-7

Liu, Y., & Whitman, W. B. (2008). Metabolic, phylogenetic, and ecological diversity of the methanogenic archaea. *Annals of the New York Academy of Sciences*, 1125(1), 171–189. https://doi.org/10.1196/annals.1419.019

Lyu, Z., Shao, N., Akinyemi, T., & Whitman, W. B. (2018). Methanogenesis. *Current Biology*, 28(13), R727–R732. https://doi.org/10.1016/j.cub.2018.05.021

Maltby, J., Steinle, L., Löscher, C. R., Bange, H. W., Fischer, M. A., Schmidt, M., & Treude, T. (2018). Microbial methanogenesis in the sulfate-reducing zone of sediments in the Eckernförde Bay, SW Baltic Sea. *Biogeosciences*, 15(1), 137–157. https://doi.org/10.5194/bg-15-137-2018

Martinez-Cruz, K., Leewis, M. C., Herriott, I. C., Sepulveda-Jauregui, A., Anthony, K. W., Thalasso, F., & Leigh, M. B. (2017). Anaerobic oxidation of methane by aerobic methanotrophs in sub-Arctic lake sediments. *Science of the Total Environment*, 607-608, 23–31. https://doi.org/10.1016/j.scitotenv.2017.06.187

Marzi, R., Torkelson, B. E., & Olson, R. K. (1993). A revised carbon preference index. *Organic Geochemistry*, 20(8), 1303–1306. https://doi.org/10.1016/0146-6380(93)90016-5

Mitterer, R. M. (2010). Methanogenesis and sulfate reduction in marine sediments: A new model. *Earth and Planetary Science Letters*, 295(3–4), 358–366. https://doi.org/10.1016/j.epsl.2010.04.009

Myhre, G., Shindell, D., Bréon, F., Collins, W., Fuglestvedt, J., Huang, J., Koch, D., Lamarque, J., Lee, D., & Mendoza, B. (2013). Anthropogenic and natural radiative forcing, climate change 2013: The physical science basis. In T. F. Stocker, D. Qin, G.-K. Plattner, M. Tignor, S. K. Allen, J. Boschung, A. Nauels, Y. Xia, V. Bex, & P. M. Midgley (Eds.), *Contribution of working group I to the fifth assessment report of the intergovernmental panel on climate change* (pp. 659–740). Cambridge University Press.

Nakamura, F. M. (2019). *Microcosms and the role of active microbiota on methane cycle in soils under forest and pasture of eastern Amazon.* Universidade de São Paulo.

Nauhaus, K., Boetius, A., Kruger, M., & Widdel, F. (2002). In vitro demonstration of anaerobic oxidation of methane coupled to sulphate reduction in sediment from a marine gas hydrate area. *Environmental Microbiology*, 4(5), 296–305. https://doi.org/10.1046/j.1462-2920.2002.00299.x

Nurk, S., Meleshko, D., Korobeynikov, A., & Pevzner, P. A. (2017). metaSPAdes: A new versatile metagenomic assembler. *Genome Research*, 27(5), 824–834. https://doi.org/10.1101/gr.213959.116

Oksanen, J., Blanchet, F. G., Friendly, M., Kindt, R., Legendre, P., McGlinn, D., Minchin, P. R., O'Hara, R. B., Simpson, G. L., Solymos, P., Stevens, M. H. H., Szoecs, E., & Wagner, H. (2019). *Vegan: Community ecology package. R Package Version 2.5-6.* https://CRAN.R-project.org/package=vegan

Olefeldt, D., Goswami, S., Grosse, G., Hayes, D., Hugelius, G., Kuhry, P., McGuire, A. D., Romanovsky, V. E., Sannel, A. B., Schuur, E. A., & Turetsky, M. R. (2016). Circumpolar distribution and carbon storage of thermokarst landscapes. *Nature Communications*, 7(1), 13043. https://doi.org/10.1038/ncomms13043

Oswald, K., Graf, J. S., Littmann, S., Tienken, D., Brand, A., Wehrli, B., Albertsen, M., Daims, H., Wagner, M., Kuypers, M. M., Schubert, C. J., & Milucka, J. (2017). Crenothrix are major methane consumers in stratified lakes. *The ISME Journal*, 11(9), 2124–2140. https://doi.org/10.1038/ismej.2017.77

Ozuolmez, D., Moore, E. K., Hopmans, E. C., Sinninghe Damste, J. S., Stams, A. J. M., & Plugge, C. M. (2020). Butyrate conversion by sulfate-reducing and methanogenic communities from anoxic sediments of Aarhus Bay, Denmark. *Microorganisms*, 8(4), 606. https://doi.org/10.3390/microorganisms8040606

Ozuolmez, D., Na, H., Lever, M. A., Kjeldsen, K. U., Jorgensen, B. B., & Plugge, C. M. (2015). Methanogenic archaea and sulfate reducing bacteria co-cultured on acetate: Teamwork or coexistence? *Frontiers in Microbiology*, 6, 492. https://doi.org/10.3389/fmicb.2015.00492

Patzner, M. S., Logan, M., McKenna, A. M., Young, R. B., Zhou, Z., Joss, H., Mueller, C. W., Hoeschen, C., Scholten, T., Straub, D., Kleindienst, S., Borch, T., Kappler, A., & Bryce, C. (2022). Microbial iron cycling during palsa hillslope collapse promotes greenhouse gas emissions before complete permafrost thaw. *Communications Earth & Environment*, 3(1), 76. https://doi.org/10.1038/s43247-022-00407-8

Pellerin, A., Lotem, N., Walter Anthony, K., Eliani Russak, E., Hasson, N., Roy, H., Chanton, J. P., & Sivan, O. (2022). Methane production controls in a young thermokarst lake formed by abrupt permafrost thaw. *Global Change Biology*, 28(10), 3206–3221. https://doi.org/10.1111/gcb.16151

Penger, J., Conrad, R., & Blaser, M. (2012). Stable carbon isotope fractionation by methylotrophic methanogenic archaea. *Applied and Environmental Microbiology*, 78(21), 7596–7602. https://doi.org/10.1128/AEM.01773-12

Pohlman, J. W., Riedel, M., Bauer, J. E., Canuel, E. A., Paull, C. K., Lapham, L., Grabowski, K. S., Coffin, R. B., & Spence, G. D. (2013). Anaerobic methane oxidation in low-organic content methane seep sediments. *Geochimica et Cosmochimica Acta*, 108, 184–201. https://doi.org/10.1016/j.gca.2013.01.022

Rooze, J., Egger, M., Tsandev, I., & Slomp, C. P. (2016). Iron-dependent anaerobic oxidation of methane in coastal surface sediments: Potential controls and impact. *Limnology and Oceanography*, 61(S1), S267–S282. https://doi.org/10.1002/lno.10275

Rosseel, Y. (2012). Lavaan: An R package for structural equation modeling. *Journal of Statistical Software*, 48(2), 1–36.

Sansone, F. J., & Martens, C. S. (1981). Methane production from acetate and associated methane fluxes from anoxic coastal sediments. *Science*, 211(4483), 707–709. https://doi.org/10.1126/science.211.4483.707

Schindler, M. (2019). *Microbial process rates in thermokarst lake sediments from Bykovsky Peninsula, Northern Siberia.* University of Tübingen, Tübingen.

Schink, B. (2010). Anaerobic transformation processes, microbiology. In J. Reitner & V. Thiel (Eds.), *Encyclopedia of Geobiology* (pp. 48–52). Springer.

Schirrmeister, L., Grigoriev, M. N., Strauss, J., Grosse, G., Overduin, P. P., Kholodov, A., Guenther, F., & Hubberten, H.-W. (2018). Sediment characteristics of a thermokarst lagoon in the northeastern Siberian Arctic (Ivashkina lagoon Bykovsky Peninsula). *Arktos*, 4(1), 1–16. https://doi.org/10.1007/s41063-018-0049-8

Schuur, E. A., McGuire, A. D., Schadel, C., Grosse, G., Harden, J. W., Hayes, D. J., Hugelius, G., Koven, C. D., Kuhry, P., Lawrence, D. M., Natali, S. M., Olefeldt, D., Romanovsky, V. E., Schaefer, K., Turetsky, M. R., Treat, C. C., & Vonk, J. E. (2015). Climate change and the permafrost carbon feedback. *Nature*, 520(7546), 171–179. https://doi.org/10.1038/nature14338

Sela-Adler, M., Ronen, Z., Herut, B., Antler, G., Vigderovich, H., Eckert, W., & Sivan, O. (2017). Co-existence of Methanogenesis and sulfate reduction with common substrates in sulfate-Rich estuarine sediments. *Frontiers in Microbiology*, 8(766), 766. https://doi.org/10.3389/fmicb.2017.00766

Serikova, S., Pokrovsky, O. S., Laudon, H., Krickov, I. V., Lim, A. G., Manasypov, R. M., & Karlsson, J. (2019). High carbon emissions from thermokarst lakes of Western Siberia. *Nature Communications*, 10(1), 1552. https://doi.org/10.1038/s41467-019-09592-1

Sollinger, A., & Urich, T. (2019). Methylotrophic methanogens everywhere—physiology and ecology of novel players in global methane cycling. *Biochemical Society Transactions*, 47(6), 1895–1907. https://doi.org/10.1042/BST20180565

Spangenberg, I., Overduin, P. P., Damm, E., Bussmann, I., Meyer, H., Liebner, S., Angelopoulos, M., Biskaborn, B. K., Grigoriev, M. N., & Grosse, G. (2021). Methane pathways in winter ice of a thermokarst lake–lagoon–coastal water transect in North Siberia. *The Cryosphere*, 15(3), 1607–1625. https://doi.org/10.5194/tc-15-1607-2021

Strauss, J., Abbott, B., Hugelius, G., Schuur, E. A. G., Treat, C., Fuchs, M., Schädel, C., Ulrich, M., Turetsky, M. R., Keuschnig, M., Biasi, C., Yang, Y., & Grosse, G. (2021). Permafrost. In FAO & ITPS (Ed.), *Recarbonizing global soils—A technical manual of recommended management*

practices (Vol. 2, p. 251). Food & Agriculture Organization. https://doi.org/10.4060/cb6378en

Strauss, J., Schirrmeister, L., Grosse, G., Fortier, D., Hugelius, G., Knoblauch, C., Romanovsky, V., Schädel, C., Schneider von Deimling, T., Schuur, E. A. G., Shmelev, D., Ulrich, M., & Veremeeva, A. (2017). Deep Yedoma permafrost: A synthesis of depositional characteristics and carbon vulnerability. *Earth-Science Reviews*, 172, 75–86. https://doi.org/10.1016/j.earscirev.2017.07.007

Su, Y., Zheng, X., Chen, Y., Li, M., & Liu, K. (2015). Alteration of intracellular protein expressions as a key mechanism of the deterioration of bacterial denitrification caused by copper oxide nanoparticles. *Scientific Reports*, 5, 15824. https://doi.org/10.1038/srep15824

Thomsen, T. R., Finster, K., & Ramsing, N. B. (2001). Biogeochemical and molecular signatures of anaerobic methane oxidation in a marine sediment. *Applied and Environmental Microbiology*, 67(4), 1646–1656. https://doi.org/10.1128/AEM.67.4.1646-1656.2001

Timmers, P. H., Widjaja-Greefkes, H. C., Ramiro-Garcia, J., Plugge, C. M., & Stams, A. J. (2015). Growth and activity of ANME clades with different sulfate and sulfide concentrations in the presence of methane. *Frontiers in Microbiology*, 6, 988. https://doi.org/10.3389/fmicb.2015.00988

Tokida, T., Miyazaki, T., Mizoguchi, M., & Seki, K. (2005). In situ accumulation of methane bubbles in a natural wetland soil. *European Journal of Soil Science*, 56(3), 389–396. https://doi.org/10.1111/j.1365-2389.2004.00674.x

Turetsky, M. R., Abbott, B. W., Jones, M. C., Anthony, K. W., Olefeldt, D., Schuur, E. A. G., Grosse, G., Kuhry, P., Hugelius, G., Koven, C., Lawrence, D. M., Gibson, C., Sannel, A. B. K., & McGuire, A. D. (2020). Carbon release through abrupt permafrost thaw. *Nature Geoscience*, 13(2), 138–143. https://doi.org/10.1038/s41561-019-0526-0

Versantvoort, W., Guerrero-Cruz, S., Speth, D. R., Frank, J., Gambelli, L., Cremers, G., van Alen, T., Jetten, M. S. M., Kartal, B., Op den Camp, H. J. M., & Reimann, J. (2018). Comparative genomics of Candidatus Methylomirabilis species and description of Ca. Methylomirabilis Lanthanidiphila. *Frontiers in Microbiology*, 9, 1672. https://doi.org/10.3389/fmicb.2018.01672

Viollier, E., Inglett, P. W., Hunter, K., Roychoudhury, A. N., & Van Cappellen, P. (2000). The ferrozine method revisited: Fe(II)/Fe(III) determination in natural waters. *Applied Geochemistry*, 15(6), 785–790. https://doi.org/10.1016/s0883-2927(99)00097-9

Vyse, S. A., Herzschuh, U., Andreev, A. A., Pestryakova, L. A., Diekmann, B., Armitage, S. J., & Biskaborn, B. K. (2020). Geochemical and sedimentological responses of arctic glacial Lake Ilirney, chukotka (far East Russia) to palaeoenvironmental change since ~51.8 ka BP. *Quaternary Science Reviews*, 247, 106607. https://doi.org/10.1016/j.quascirev.2020.106607

Vyse, S. A., Herzschuh, U., Pfalz, G., Pestryakova, L. A., Diekmann, B., Nowaczyk, N., & Biskaborn, B. K. (2021). Sediment and carbon accumulation in a glacial lake in Chukotka (Arctic Siberia) during the late Pleistocene and Holocene: Combining hydroacoustic profiling and down-core analyses. *Biogeosciences*, 18(16), 4791–4816. https://doi.org/10.5194/bg-18-4791-2021

Wagner, D., Lipski, A., Embacher, A., & Gattinger, A. (2005). Methane fluxes in permafrost habitats of the Lena Delta: Effects of microbial community structure and organic matter quality. *Environmental Microbiology*, 7(10), 1582–1592. https://doi.org/10.1111/j.1462-2920.2005.00849.x

Wallenius, A. J., Dalcin Martins, P., Slomp, C. P., & Jetten, M. S. M. (2021). Anthropogenic and environmental constraints on the microbial methane cycle in coastal sediments. *Frontiers in Microbiology*, 12, 631621. https://doi.org/10.3389/fmicb.2021.631621

Walter Anthony, K., Daanen, R., Anthony, P., Schneider von Deimling, T., Ping, C.-L., Chanton, J. P., & Grosse, G. (2016). Methane emissions proportional to permafrost carbon thawed in Arctic lakes since the 1950s. *Nature Geoscience*, 9, 679–682. https://doi.org/10.1038/ngeo2795

Walter Anthony, K., Schneider von Deimling, T., Nitze, I., Frolking, S., Emond, A., Daanen, R., Anthony, P., Lindgren, P., Jones, B., & Grosse, G. (2018). 21st-century modeled permafrost carbon emissions accelerated by abrupt thaw beneath lakes. *Nature Communications*, 9(1), 3262. https://doi.org/10.1038/s41467-018-05738-9

Walter, K. M., Edwards, M. E., Grosse, G., Zimov, S. A., & Chapin, F. S., 3rd. (2007). Thermokarst lakes as a source of atmospheric CH4 during the last deglaciation. *Science*, 318(5850), 633–636. https://doi.org/10.1126/science.1142924

Walz, J., Knoblauch, C., Tigges, R., Opel, T., Schirrmeister, L., & Pfeiffer, E.-M. (2018). Greenhouse gas production in degrading ice-rich permafrost deposits in northeastern Siberia. *Biogeosciences*, 15(17), 5423–5436. https://doi.org/10.5194/bg-15-5423-2018

Weil, M., Wang, H., Bengtsson, M., Köhn, D., Günther, A., Jurasinski, G., Couwenberg, J., Negassa, W., Zak, D., & Urich, T. (2020). Long-term rewetting of three formerly drained peatlands drives congruent compositional changes in pro-and eukaryotic soil microbiomes through environmental filtering. *Microorganisms*, 8(4), 550.

Wen, X., Unger, V., Jurasinski, G., Koebsch, F., Horn, F., Rehder, G., Sachs, T., Zak, D., Lischeid, G., & Knorr, K.-H. (2018). Predominance of methanogens over methanotrophs in rewetted fens characterized by high methane emissions. *Biogeosciences*, 15(21), 6519–6536.

Wickham, H. (2016). *ggplot2: Elegant graphics for data analysis*. Springer-Verlag New York http://ggplot2.org

Wiesenburg, D. A., & Guinasso, N. L. (2002). Equilibrium solubilities of methane, carbon monoxide, and hydrogen in water and sea water. *Journal of Chemical & Engineering Data*, 24(4), 356–360. https://doi.org/10.1021/je60083a006

Winkel, M., Mitzscherling, J., Overduin, P. P., Horn, F., Winterfeld, M., Rijkers, R., Grigoriev, M. N., Knoblauch, C., Mangelsdorf, K., Wagner, D., & Liebner, S. (2018). Anaerobic methanotrophic communities thrive in deep submarine permafrost. *Scientific Reports*, 8(1), 1291. https://doi.org/10.1038/s41598-018-19505-9

Xiao, K. Q., Beulig, F., Røy, H., Jørgensen, B. B., & Risgaard-Petersen, N. (2018). Methylotrophic methanogenesis fuels cryptic methane cycling in marine surface sediment. *Limnology and Oceanography*, 63(4), 1519–1527. https://doi.org/10.1002/lno.10788

Yang, S. (2020). otuSummary: Summarizing OTU table regarding the composition, abundance and beta diversity of abundant and rare biospheres. verion 0.1.1. https://github.com/cam315/otuSummary

Yang, S., Anthony, S. E., Jenrich, M., In 't Zandt, M. H., Strauss, J., Overduin, P. P., Grosse, G., Angelopoulos, M., Biskaborn, B. K., Grigoriev, M. N., Wagner, D., Knoblauch, C., Jaeschke, A., Rethemeyer, J., Kallmeyer, J., & Liebner, S. (2022a). *Sequencing data of sediments from Arctic thermokarst lakes and lagoons on the Bykovsky Peninsula, Siberia*. https://www.ebi.ac.uk/ena/browser/view/PRJEB49195

Yang, S., Anthony, S. E., Jenrich, M., In 't Zandt, M. H., Strauss, J., Overduin, P. P., Grosse, G., Angelopoulos, M., Biskaborn, B. K., Grigoriev, M. N., Wagner, D., Knoblauch, C., Jaeschke, A., Rethemeyer, J., Kallmeyer, J., & Liebner, S. (2022b). *Geochemistry of sediments from Arctic thermokarst lakes and lagoons on the Bykovsky Peninsula, Siberia*. https://doi.org/10.5880/GFZ.3.7.2022.001

Yang, S., Liebner, S., Svenning, M. M., & Tveit, A. T. (2021). Decoupling of microbial community dynamics and functions in Arctic peat soil exposed to short term warming. *Molecular Ecology*, 30(20), 5094–5104. https://doi.org/10.1111/mec.16118

Zalman, C. A., Meade, N., Chanton, J., Kostka, J. E., Bridgham, S. D., & Keller, J. K. (2018). Methylotrophic methanogenesis in

sphagnum-dominated peatland soils. *Soil Biology and Biochemistry*, *118*, 156–160. https://doi.org/10.1016/j.soilbio.2017.11.025

Zheng, Y., Zhou, W., Meyers, P. A., & Xie, S. (2007). Lipid biomarkers in the Zoigê-Hongyuan peat deposit: Indicators of holocene climate changes in West China. *Organic Geochemistry*, *38*(11), 1927–1940. https://doi.org/10.1016/j.orggeochem.2007.06.012

SUPPORTING INFORMATION

Additional supporting information can be found online in the Supporting Information section at the end of this article.